IEICE TRANS. COMMUN., VOL.E107–B, NO.6 JUNE 2024

PAPER

Physical Layer Security Enhancement for mmWave System with Multiple RISs and Imperfect CSI

Qingqing TU[†*a)], ***Member***, **Zheng DONG**[††], **Xianbing ZOU**[†], ***and*** **Ning WEI**[†], ***Nonmembers***

SUMMARY Despite the appealing advantages of reconfigurable intelligent surfaces (RIS) aided mmWave communications, there remain practical issues that need to be addressed before the large-scale deployment of RISs in future wireless networks. In this study, we jointly consider the non-neglectable practical issues in a multi-RIS-aided mmWave system, which can significantly affect the secrecy performance, including the high computational complexity, imperfect channel state information (CSI), and finite resolution of phase shifters. To solve this non-convex challenging stochastic optimization problem, we propose a robust and low-complexity algorithm to maximize the achievable secrete rate. Specially, by combining the benefits of fractional programming and the stochastic successive convex approximation techniques, we transform the joint optimization problem into some convex ones and solve them sub-optimally. The theoretical analysis and simulation results demonstrate that the proposed algorithms could mitigate the joint negative effects of practical issues and yielded a trade-off between secure performance and complexity/overhead outperforming non-robust benchmarks, which increases the robustness and flexibility of multiple RIS deployments in future wireless networks.

key words: *reconfigurable intelligent surfaces (RIS), physical layer security, millimeter wave (mmWave), imperfect CSI, robust beamforming*

1. Introduction

The millimeter wave (mmWave) communications can significantly boost network capacity to make ubiquitous and on-demand interconnection possible in future wireless networks [1]–[3]. However, owing to the propagation loss of the mmWave band and the broadcast nature of wireless channels, mmWave communication suffers from the risk of information leakage in the presence of eavesdroppers, especially when the legitimate and wiretap channels are highly correlated, which makes security an indispensable pursuit for system development. In this context, physical layer security (PLS) has drawn significant research interest in recent years [4], [5]. Compared with traditional cryptography, the PLS techniques enable secrecy communication independently of the higher layers by taking advantage of the inherent randomness of noise and communication channels, such as cooperative relaying schemes, artificial noise-aided beamforming, and cooperative jamming [6]–[9]. However, enhancing the PLS by deploying a large number of relays or other active nodes will inevitably increase the cost and complexity of the communication systems. To solve this problem, reconfigurable intelligent surfaces (RIS) have recently been introduced to provide a new paradigm for the PLS enhancement [10], [11]. Unlike active components that formulate active beamforming to transmit signal, such as base stations, the RIS achieves passive beamforming through its passive planar surface. This surface consists of a large number of passive reflecting elements, each capable of inducing a controllable amplitude [12] and/or phase [13] changes to the incident signal. Thus, it incurs lower energy costs compared to active antenna arrays. With this property, the RIS can serve as an auxiliary device flexibly deployed in wireless networks to boost or suppress the received signals and also improve the network coverage by creating virtual LOS links, especially in the higher frequency bands like mmWave [14] to deal with the severe path loss and the signal blockage problem. These unique merits stimulate the increasing interest in RIS-aided PLS enhancement research. As illustrated in [15]–[17], the secure performance is investigated in the RIS-aided wireless communication systems with both legitimate receivers and eavesdroppers existing. By developing various non-convex optimization techniques, such as the successive convex approximation (SCA)-based method, the semidefinite relaxation (SDR)-based method, and the manifold optimization (MO)-based method, it revealed that the secure performance of the system with RIS outperforms the case without RIS, which proves the advantage of deployment of the RIS in the secure transmission.

However, the low-rank channel of a single RIS to AP is hard to support secure transmissions in the existence of eavesdroppers, especially when the wiretap channel is stronger than the legitimate user channel. To conquer this issue, multiple RIS deployment is investigated to further enhance the secure performance of ubiquitous wireless networks [18], [19]. Furthermore, the benefits brought by the multiple RIS deployment also perfectly match with the secure mmWave communications. To circumvent the inherent disadvantages of mmWave, typical multiple-input multiple-output (MIMO) technologies with massive array antennas are deployed to cope with the high path-loss problem [20]–[22]. However, continuous increment in antenna number is impractical due to the high hardware complexity and power consumption [23] and the blockage-prone issue has still not been well addressed. A more feasible solution is to in-

Manuscript received October 21, 2023.
Manuscript publicized January 30, 2024.

[†]The authors are with the National Key Laboratory of Science and Technology on Communications, University of Electronic Science and Technology of China, Chengdu 611731, China.
[††]The author is with the School of Information Science and Engineering, Shandong University, Qingdao, 266237, Shandong Province, China.
[*]Presently, with the National Computer Network Emergency Response Technical Team/Coordination Center of China.
a) E-mail: tuqingqing@cert.org.cn

DOI: 10.23919/transcom.2023EBP3169

troduce distributed RISs to aid secure communication in the mmWave system, which provides a more cost-efficient way to compensate for the limited secure propagation distance problem by forming virtual line-of-sight (LoS) paths as proved in [24], [25]. By jointly optimizing active and passive beamformers, the author in [26] maximized the secrecy rate and proved the significant secure performance gains offered by the multiple RISs deployment when the eavesdropper exists. However, the multi-RIS-aided PLS enhancement performance for the mmWave system is still restricted by practical issues.

The first challenging issue lies in the acquisition of accurate channel state information (CSI) of the RIS due to its passive operation and a large number of reflecting elements. In general, the performance of the joint optimization for passive beamforming and active beamforming is highly dependent on the quality of the acquired CSI. Despite the various methods for the RIS channel estimation [27]–[29], the estimation error is still inevitable because of the channel background noise, time-varying characteristics, and more importantly, the fundamental limitation of no active transmitting elements on the RIS [30]. Although the previous works on RIS aided secure transmission treating the estimated channels as perfect ones achieved encouraging results, it will inevitably lead to system performance loss and weaken the generality and practicality of the systems and algorithms. Hence, it is crucial to consider the CSI uncertainties for the RIS-aided PLS enhancement scheme. In the recent work to deal with the imperfect CSI problem, one way is to introduce artificial noise (AN) to deliberately destroy the wiretap channel and reduce the dependency on CSI by optimizing the power fraction of AN and the RIS phase shifts [31]–[33]. However, the extra power is located to transmit the AN signal, which is not cost-efficient. Another way is to use the imperfect CSI to design the joint beamforming in the RIS-aided system. To model the uncertain CSI error, the bounded error model is commonly used in existing works [34]–[36], which proposed a worst-case robust beamforming design and obtained a suboptimal solution by setting the channel quantization error within a bounded region. However, this model may not adapt to apply in the realistic channel, since the estimation error is Gaussian due to the linear channel estimator under Gaussian noise. This problem can be handled in the Gaussian CSI error model (or statistical CSI error model), which could introduce stochastic optimization in the secure design for RIS-aided networks. Specifically, the authors in [30] showed that better performance could be obtained in a robust beamforming design under this type of CSI error model in terms of convergence speed and complexity. To make the secure transmission design more practical, the authors of [37]–[40] investigated different performance metrics for RIS-aided systems under imperfect CSI of eavesdroppers, such as the average secrecy rate, energy efficiency, and secrecy outage probability, which proposed different algorithms to improve the security performance. However, we note that all these secure works only considered the scenarios with the imperfect CSI of the eavesdroppers, while no relevant research on analyzing the secure performance of multi-RIS-aided systems considering imperfect CSI of both intended users and eavesdroppers, which is more practical. Moreover, compared with the previous work, this optimization problem is more difficult to solve, and the converged solution under alternating optimization iteration is uncertain due to the random system states introduced by the imperfect CSI of both the intended user and the eavesdropper. Hence, due to the lack of adequate material in the literature, the secure performance of multiple RISs in mmWave systems under such imperfect CSI cases is yet to be explored and utilized up to their full potential.

The second non-neglectable practical issue is the high computational complexity in multi-RIS-aided systems due to the large-scale reflection coefficients optimization [41]. The number of reflection elements on RIS is typically much larger than that of the antennas on the access point (AP), and the reflection coefficients optimization on the RISs is computationally prohibitive, especially when multiple RISs are deployed. In addition, the complex methods applied to address the non-convex joint optimization problem result in increased complexity, such as the SDR-based method [13], SCA-based method [42], and MO-based method [26], [43], which will further restrict the realization of the full potential of RIS. Thus, reducing the computational complexity of joint beamforming design is essential for the practical deployment of multiple RISs.

The third practical issue is the adoption of phase shifters with a finite resolution on the RIS to strike a balance between hardware cost and system performance. For simplicity, many aforementioned RIS-aided security schemes implicitly assume that infinite-resolution phase shifters are available on the RIS, which are arguably prohibitive to implement [44]. On the other hand, applying finite-resolution phase shifters will inevitably incur a notable secrecy performance loss [41]. Previous studies have focused on addressing issues such as transmitted power minimization, sum-rate maximization, and coverage improvement using the finite-resolution phase shifters in the specific terminal settings [45]–[48], which encompass parameters like RIS size, power constraint, rate constraint. The work in [48] further investigated the required number of phase shifts under a rate constraint. Nevertheless, the RIS-aided PLS enhancement scheme under the finite-resolution phase shifters case still needs further investigation.

In summary, with the increased demands for the RIS deployment scale in the future, it is worth extending the secure transmission designs to more practical setups in the mmWave systems. However, jointly considering these non-neglectable practical issues leads to a more challenging stochastic optimization due to more coupled variables, complex objective functions, non-convex constraints, and random system states. To our best knowledge, this is still an open problem and requires new solution approaches.

In this paper, we consider an mmWave system with multiple RISs deployed against eavesdroppers and investi-

gate the secrecy performance gain jointly affected by these practical issues. To address this challenging non-convex stochastic optimization problem, we propose a robust and low-complexity method to provide trade-offs concerning secrecy performance, complexity, and cost. The main contributions of this paper are summarized as follows.

- We formulate a robust secure beamforming problem to maximize the worst-case achievable SR under the joint effects of non-neglectable practical issues. Different from the existing RIS-aided work under the imperfect CSI of eavesdroppers [37]–[40], our design simultaneously considers the imperfect CSI of both intended users and eavesdroppers and also expanded to the low-resolution shifters case.
- To solve this challenging non-convex stochastic optimization problem, we expressed the imperfect CSI model with the random system states and propose robust and low-complexity methods to transform the objective problem into simplified and convex subproblems by combining the benefits of the fractional programming and the stochastic successive convex approximation techniques. We mathematically prove that the convergence conditions are satisfied in each subproblem optimization, and the resulting achievable SR under alternating optimization iteration is guaranteed to converge.
- The proposed method exhibits a robustness improvement over the non-robust benchmarks and achieves a close secure performance gain to that of perfect CSI performance when the estimation error is bounded, while at a lower computational complexity via theoretical analysis and simulations. Furthermore, the RIS of 3-bit phase adjustable elements achieves the equivalent value as the continuous phase shift. These proved that the proposed method can reduce the demand for perfect CSI and infinite hardware resolution, which increases the flexibility and robustness of multiple RIS deployment in various practical scenarios.

Notations: Variables, vectors, and matrices are respectively written as lower-case letters, bold lower-case letters and bold upper-case letters. $\mathbf{A}_{m,n}$ is the the m-th row and n-th column element of the matrix $\mathbf{A}$. $\mathrm{tr}(\cdot)$, $(\cdot)^T$, and $(\cdot)^H$ stand for the trace, the transpose, and the conjugate transpose, respectively, while $(\cdot)^*$ donates the conjugate. $\|\cdot\|$ and $\|\cdot\|_F$ is the Euclidean norm and the Frobenius norm of a complex vector and matrix, respectively. $\mathrm{diag}(\cdot)$ represents the diagonal matrix whose diagonals are the elements of the input vector. j denotes the imaginary unit. $[\cdot]_{(1:m)}$ returns the vector that contains the first m elements. Finally, $\log(x)$ represents base 2 logarithm of x.

2. System Model and Problem Formulation

This section describes a multi-RIS-aided downlink mmWave system with both the intended user and eavesdropper. In addition, the channel model, which considers the CSI uncertainties, is also discussed.

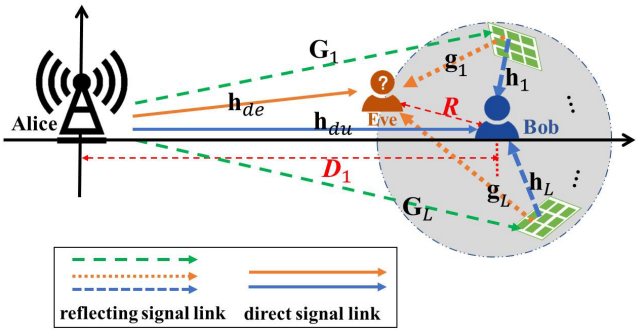

Fig. 1 The multi-RIS-aided secure mmWave system.

2.1 System Model

We consider the downlink of a TDD-based multi-RIS-aided mmWave system where the eavesdropper (Eve) attempts to eavesdrop on the confidential message sent from an access point (Alice) to the receiver (Bob), which is under a worst-case assumption that near-end Eve tries to intercept the information of far-end Bob, which could lead to the zero secrecy rate (SR) problem [41]. Specially, we assume that both Eve and Bob are regular users of the system and hence know the communication protocols. In addition, a set of L RISs are distributively deployed [49] to enhance the SR as well as the network coverage by reflecting the received signals, as depicted in Fig. 1.

We assume that Alice has N antennas, and each RIS is equipped with $M = M_1 \times M_2$ reflecting elements arranged in a uniform planer array (UPA) with M_1 elements horizontally and M_2 elements vertically. Following [41], the phase shifter matrix of the l-th RIS is $\mathbf{\Theta}_l = \mathrm{diag}(\boldsymbol{\theta}_l) \in \mathbb{C}^{M\times M}$, $\boldsymbol{\theta}_l = \sqrt{\eta}[\theta_{1,l}, \cdots, \theta_{M,l}]^T$, in which η is the amplitude reflection coefficient, and $\theta_{m,l} = e^{j\phi_{m,l}}, m = 1, \cdots, M, l \in \mathcal{L}$. We can adjust the phase shifts $\phi_{m,l} \in [0, 2\pi)$ of each reflecting element to create a virtual line-of-sight (LoS) link.

The channel matrix between Alice and the l-th RIS is represented by $\mathbf{G}_l \in \mathbb{C}^{M\times N}$. The channel vector between the l-th RIS and Bob is denoted by $\mathbf{h}_l \in \mathbb{C}^{M\times 1}$, while $\mathbf{g}_l \in \mathbb{C}^{M\times 1}$ is the channel vector between the l-th RIS and Eve. The LoS channel vectors, the Alice-Bob link and the Alice-Eve link, are represented by $\mathbf{h}_{du} \in \mathbb{C}^{N\times 1}$ and $\mathbf{h}_{de} \in \mathbb{C}^{N\times 1}$, respectively. Now, the received signal at Bob over the cascaded channel via the RIS can be modeled by

$$y_u = \left(\sum_{l=1}^{L} \mathbf{h}_l^H \mathbf{\Theta}_l \mathbf{G}_l + \mathbf{h}_{du}^H\right) \mathbf{w} s + n, \tag{1}$$

where s is the confidential transmitted signal such that $\mathbb{E}[|s|^2] = 1$, and $\mathbf{w} \in \mathbb{C}^{N\times 1}$ is the beamforming vector subject to a total transmit power constraint $\mathrm{tr}(\mathbf{w}\mathbf{w}^H) \le P$. In addition, $n \sim \mathcal{CN}(0, \sigma^2)$ is an additive zero-mean Gaussian noise at Bob. Likewise, the signal received at Eve can be given by

$$y_e = \left(\sum_{l=1}^{L} \mathbf{g}_l^H \mathbf{\Theta}_l \mathbf{G}_l + \mathbf{h}_{de}^H\right)\mathbf{w}s + n_e, \tag{2}$$

where $n_e \sim \mathcal{CN}(0, \sigma_e^2)$ is the additive complex Gaussian noise at Eve. The signal-to-interference-plus-noise ratio (SINR) of the received signal of Bob is formulated by

$$\gamma_u = \frac{\|(\sum_{l=1}^{L} \mathbf{h}_l^H \mathbf{\Theta}_l \mathbf{G}_l + \mathbf{h}_{du}^H)\mathbf{w}\|^2}{\sigma^2}. \tag{3}$$

The SINR for Eve is given in a similar fashion by

$$\gamma_e = \frac{\|(\sum_{l=1}^{L} \mathbf{g}_l^H \mathbf{\Theta}_l \mathbf{G}_l + \mathbf{h}_{de}^H)\mathbf{w}\|^2}{\sigma_e^2}. \tag{4}$$

Therefore, achievable SR between Alice and Bob can be written as

$$R_s(\mathbf{w}, \mathbf{\Theta}) = \left[\log(1+\gamma_u) - \log(1+\gamma_e)\right]^+, \tag{5}$$

where $[x]^+ \triangleq \max\{0, x\}$. It is worth pointing out that the optimal value of R_s is always non-negative by adjusting the beamforming vectors. This can be shown by contradiction. If we assume that the optimal value $R_s(\mathbf{w}^*, \mathbf{\Theta}^*)$ is negative and $\mathbf{w}^*$ is the optimal value. Then, by setting $\|\mathbf{w}\| = 0$, we can obtain $R_s = 0$, which contradicts our assumption.

2.2 Channel Model

In our system, there are two types of channels: the direct channel between Alice and Bob (or Eve) $\mathbf{h}_{d,i}, i = \{u, e\}$, and the RIS-aided cascaded channel $\mathbf{G}$, $\mathbf{g}$, and $\mathbf{h}$. We assume that the direct channel $\mathbf{h}_{d,i}, i = \{u, e\}$ with rich scatters are Rayleigh distributed, while the channel $\mathbf{G}$, $\mathbf{g}$, and $\mathbf{h}$ follow a Rician fading, since the LoS components are generally contained in the RIS-aided cascaded channel, which is similar to the model described in [40], [43], [50]. More specifically, the Alice-to-RIS, the RIS-to-Bob, and the RIS-to-Eve mmWave channels are expressed as followed

$$\mathbf{G} = \left(\sqrt{\frac{\kappa_1}{\kappa_1+1}}\bar{\mathbf{G}} + \sqrt{\frac{1}{\kappa_1+1}}\hat{\mathbf{G}}\right)L_{AR}, \tag{6a}$$

$$\mathbf{h} = \left(\sqrt{\frac{\kappa_2}{\kappa_2+1}}\bar{\mathbf{h}} + \sqrt{\frac{1}{\kappa_2+1}}\hat{\mathbf{h}}\right)L_{RU}, \tag{6b}$$

$$\mathbf{g} = \left(\sqrt{\frac{\kappa_3}{\kappa_3+1}}\bar{\mathbf{g}} + \sqrt{\frac{1}{\kappa_3+1}}\hat{\mathbf{g}}\right)L_{RE}, \tag{6c}$$

where $\bar{\mathbf{G}}$, $\bar{\mathbf{h}}$ and $\bar{\mathbf{g}}$ are the corresponding LoS components, which remains unchanged within the channel coherence time. The Rician factors in each channel are represented by $\kappa_1, \kappa_2, \kappa_3$, respectively. Also, $\hat{\mathbf{G}}, \hat{\mathbf{h}}, \hat{\mathbf{g}}$ are the channel error terms corresponding to the non-line-of-sight (NLoS) components, and each of their elements is i.i.d. CSCG random variable with zero mean and unit variance. The path-loss terms are captured by L_{AR}, L_{RU}, and L_{RE}.

Based on the mmWave channel model in [51], The LoS component of the channel between the Alice and the RIS with L_G scatters can be formulated by

$$\bar{\mathbf{G}} = \frac{1}{\sqrt{L_G}}\sum_{l_G=1}^{L_G} \mathbf{u}_t\left(\varphi_{l_G}^t\right)\mathbf{u}_r\left(\psi_{l_G}^r, \varphi_{l_G}^r\right). \tag{7}$$

The array response vector at Alice is denoted by $\mathbf{u}_t$ such that

$$\mathbf{u}_t(\varphi_{l_G}^t) = \frac{1}{\sqrt{N}}\left[1, e^{j\frac{2\pi d}{\lambda_c}\sin\left(\varphi_{l_G}^t\right)}, \cdots, e^{-j(N-1)\frac{2\pi d}{\lambda_c}\sin\left(\varphi_{l_G}^t\right)}\right], \tag{8}$$

where λ_c is the wavelength, d is the antenna spacing, and $\varphi_{l_G}^t \in [0, 2\pi)$ represents the angle of departure. For a typical UPA, array response at RIS $\mathbf{u}_r$ is expressed as

$$\begin{aligned}\mathbf{u}_r(\psi_{l_G}^r, \varphi_{l_G}^r) = &\frac{1}{\sqrt{M}}\left[1, \cdots, e^{-j\frac{2\pi d}{\lambda_c}(M_1-1)\cos\left(\varphi_{l_G}^r\right)\sin\left(\psi_{l_G}^r\right)}\right] \\ &\otimes\left[1, \cdots, e^{-j\frac{2\pi d}{\lambda_c}(M_2-1)\cos\left(\psi_{l_G}^r\right)}\right],\end{aligned} \tag{9}$$

where $\psi_{l_G}^r$ and $\varphi_{l_G}^r \in [0, 2\pi]$ represent the elevation and azimuth angle of arrival at the l-th RIS, respectively. The cascaded channel between the RISs to Bob $\mathbf{h}$ and Eve $\mathbf{g}$ is defined similarly and omitted for simplicity.

With the limited propagation range due to the strong path loss and fading effects encountered by millimeter-wave signals during transmission, the spatial correlation between the eavesdropping channel and the legitimate channel significantly influences the security performance of the system, particularly when the eavesdropper is in close proximity to the legitimate communication devices. Therefore, we introduce a correlation coefficient to describe the different spatial correlations on the receiver sides of Bob and Eve following [52], [53], which is expressed as

$$\rho_r = \frac{\mathbb{E}\{\mathbf{h}_{du}^H \mathbf{h}_{de}\}}{\sqrt{\mathbb{E}\{\mathbf{h}_{du}^H \mathbf{h}_{du}\}\mathbb{E}\{\mathbf{h}_{de}^H \mathbf{h}_{de}\}}}. \tag{10}$$

Therefore, the RIS-to-Bob and the RIS-to-Eve mmWave channels can be expressed as $\mathbf{h}_{d,i} = \sqrt{\rho_r}\mathbf{h}_{d,0} + \sqrt{1-\rho_r}\mathbf{h}_{d,i,1}$. $\mathbf{h}_{d,0}$ is the correlated component referring to the deterministic part of the channels. For $\rho_r \in [0, 1]$, $\mathbf{h}_{d,i,1}$ donates the uncorrelated components representing random variations due to fading, shadowing, and noise. When the correlation coefficient approaches 1, there is a strong spatial correlation between the eavesdropping and legitimate channels, while the spatial correlation of channels is weak when close to 0.

For our design, the CSI mismatch is taken into consideration in the joint optimization problem. Since both Bob and Eve are assumed to be regular users of the system as mentioned above, in a TDD-based transmission frame structure [43], Alice can estimate the CSI of Bob (BCSI) and the CSI of Eve (ECSI) through the transmission of pilot sequences with a linear estimator, e.g., by using a minimum mean square error (MMSE) method [54], [55]. However, the estimated BCSI and ECSI will become outdated during transmission due to the time-varying characteristics of the channel and the large number of links that need to be estimated in a multiple RISs deployed system. From the previous work, RIS mainly focuses on scenarios characterized

by low coverage and directed eavesdropping to support low-mobility users in its neighborhood, which predominantly involves slow-fading channel conditions [40], [45], [49], [56]. Following the work in [30], [40], [43], we consider the SR maximization problem under a statistical CSI error model. Through the estimation, we assume the channels expressed as

$$\mathbf{G} = \tilde{\mathbf{G}} + \Delta\mathbf{G}, \mathbf{h} = \tilde{\mathbf{h}} + \Delta\mathbf{h}, \mathbf{g} = \tilde{\mathbf{g}} + \Delta\mathbf{g}, \mathbf{h}_{di} = \tilde{\mathbf{h}}_{di} + \Delta\mathbf{h}_{di}, \quad (11)$$

where $\tilde{\mathbf{G}}$, $\tilde{\mathbf{h}}$, $\tilde{\mathbf{g}}$ and $\tilde{\mathbf{h}}_{di}$ donate the estimated channels, $i = \{u, e\}$, while $\Delta\mathbf{G}$, $\Delta\mathbf{h}$, $\Delta\mathbf{g}$ and $\Delta\mathbf{h}_{di}$ are the estimation error parts, which follow zero-mean complex Gaussian distribution. The quality of the channel estimation is indicated by $\epsilon_G = \mathbb{E}\left[||\Delta\mathbf{G}||_2^2|\tilde{\mathbf{G}}\right]$, $\epsilon_h = \mathbb{E}\left[||\Delta\mathbf{h}||_2^2|\tilde{\mathbf{h}}\right]$, $\epsilon_g = \mathbb{E}\left[||\Delta\mathbf{g}||_2^2|\tilde{\mathbf{g}}\right]$ and $\epsilon_{di} = \mathbb{E}\left[||\Delta\mathbf{h}_{di}||_2^2|\tilde{\mathbf{h}}_{di}\right]$ as considered in [30], [43], [55]. Then, to simplify the description of the uncertain channel model, we follow the methods described in [43] and define a sample space of the channels as $\mathbf{\Omega} \triangleq \{\mathbf{G}_l(\delta), \mathbf{h}_l(\delta), \mathbf{g}_l(\delta), \mathbf{h}_{di}(\delta), \forall\delta, \forall l \in \mathcal{L}\}$, based on the description of imperfect CSI and statistic CSI errors. δ denotes the index of the random realizations of $\mathbf{G}$, $\mathbf{h}$, $\mathbf{g}$, and $\mathbf{h}_{di}$ drawn from the sample space $\mathbf{\Omega}$. Specially, these realizations keep constants for varied δ when under perfect CSI setting.

2.3 Problem Formulation

In this work, we aim to maximize the achievable SR, $R_s(\mathbf{w}, \mathbf{\Theta})$ via a joint design of the active beamforming vector $\mathbf{w}$ at Alice and the passive beamforming matrix $\mathbf{\Theta}$ at the RIS. Assuming perfect CSI of Bob and Eve are available at Alice, the optimization problem is formulated by

$$\text{(P1)} \quad \max_{\mathbf{w},\mathbf{\Theta}} \quad R_s(\mathbf{w}, \mathbf{\Theta}), \quad (12a)$$

$$\text{s.t.} \quad \text{tr}(\mathbf{w}\mathbf{w}^H) \le P, \quad (12b)$$

$$\mathbf{\Theta} \in \mathcal{M}, \quad (12c)$$

where (12b) is the transmitted power constraint, and (12c) is the unit-modulus constraint on each element, i.e., $\mathcal{M} = \left\{\mathbf{\Theta} \middle| \left|\theta_{m,l}\right| = 1, \forall m = 1, \ldots, M,\ l \in \mathcal{L}\right\}$.

Next, we extend our design to a practical scenario with CSI error on both the BCSI and ECSI. Based on the channel model under imperfect CSI, we can see that the SR maximization problem is highly dependent on the random system state. From the channel model discussed above and the properties of transmission frame in RIS-aided system described in [43], [56], we assume that $\mathbf{w}$ is adaptive to the real-time CSI since the channel associate with the active beamforming $\left(\mathbf{h}_l^H\mathbf{\Theta}_l\mathbf{G}_l + \mathbf{h}_{du}^H\right) \in \mathbb{C}^{1\times N}$ with $N \ll M, l \in \mathcal{L}$, is of low-dimension. While the channel associated with the passive beamforming design $\mathbf{G}_l \,\text{diag}\,(\mathbf{h}_l) \in \mathbb{C}^{N\times M}, l \in \mathcal{L}$ is high-dimensional, which is assumed to remain approximately constant within the transmission frame and can be adjusted to the statistics of the random states. This assumption is also valid as RIS is generally used to support low-mobility users in its neighborhood [40], [45], [49], [56]. In other words, we can optimize the active beamforming and passive beamforming at different levels. The expectation of the achievable SR over the channel statistics from the sample space $\mathbf{\Omega}$ is formulated as

$$\text{(P2)} \quad \max_{\mathbf{\Theta},\{\mathbf{w}(\delta),\forall\delta\}} \quad \mathbb{E}_\delta\left[R_s\left(\mathbf{\Theta}, \mathbf{w}(\delta); \delta\right)\right], \quad (13a)$$

$$\text{s.t.} \quad \text{tr}\left(\mathbf{w}(\delta)\mathbf{w}(\delta)^H\right) \le P, \quad \forall\delta, \quad (13b)$$

$$\boldsymbol{\theta} \in \mathcal{M}. \quad (13c)$$

The problem (P2) is intractable due to the uncertain system state in the coupled variables. To tackle this problem, we decompose problem (P2) into two simplified subproblems as [57], which can be solved alternately. Based on the solution of the first subproblem associated with the current random state, the second subproblem is optimized recursively to obtain the maximum achievable SR, which results in a two-level stochastic optimization procedure as elaborated explicitly later in Sect. 4.

3. The LCFP Algorithm for Secrecy Rate Optimization

In this section, we aim to solve the SR maximization problem by taking both the computational complexity and the extension to complex scenarios into consideration.

3.1 Problem Transformation

We note that (P1) is challenging to solve, where the objective function is not jointly concave with respect to both the coupled variables $(\mathbf{w}, \mathbf{\Theta})$, and it contains the unit-modulus constraint (12c). To address the non-convex SR maximization problem with the assumption that the BCSI and ECSI are available at Alice, we aim to develop a low-complexity PLS enhancement algorithm based on the fractional programming (FP) technique, the prox-linear BCD updating technique, and the SCA method. For clarity, a summary of the algorithm, referred to as the LCFP algorithm, is given in Algorithm 1.

To deal with the logarithms and fractions parts of the

Algorithm 1 The Low-complexity Fractional Programming (LCFP) Algorithm.

1: **Input:** $t = 0$, given $\mathbf{w}^0, \boldsymbol{\theta}^0, \tau^0$.
2: **repeat**
3: Set $t = t + 1$;
4: Update the value of $a_1^{(t)}, a_2^{(t)}, \rho^{(t)}$ by (20a) (20b) (20c), and $\nabla R_s, \hat{\lambda}$ by (24) (26);
5: Obtain the optimal solution $\mathbf{w}^{(t)}$ by (25);
6: Construct $\hat{\boldsymbol{\theta}}^{(t)}, \mathbf{v}_u$ and $\mathbf{v}_e$ based on given $\mathbf{w}^{(t)}$ and $\boldsymbol{\theta}^{(t-1)}$;
6: Transform $\hat{\boldsymbol{\theta}}^{(t)}$ to $\hat{\boldsymbol{\phi}}^{(t)}$;
7: Update the $\mathbf{U}$ and $\mathbf{z}$ in (32) and (33);
8: Design step size τ using (36);
9: Update $\hat{\boldsymbol{\phi}}^{(t)}$ with (38), and transform $\hat{\boldsymbol{\phi}}^{(t)}$ to $\hat{\boldsymbol{\theta}}^{(t)}$;
10: With given $\hat{\boldsymbol{\theta}}^{(t)}$, update $\boldsymbol{\theta}^{(t)}$;
11: **Until** the stopping criterion is met.
12: **Output:** $\mathbf{w}, \boldsymbol{\theta}$.

objective function, we first reformulate the objective function by letting $R_s = R_U + R_E$, where R_U and R_E are expressed as

$$\begin{aligned} R_U &= \log\left(1 + \frac{\left\|\left(\sum_{l=1}^{L} \mathbf{h}_l^H \boldsymbol{\Theta}_l \mathbf{G}_l + \mathbf{h}_{du}^H\right)\mathbf{w}\right\|^2}{\sigma^2}\right), \\ R_E &= -\log\left(1 + \frac{\left\|\left(\sum_{l=1}^{L} \mathbf{g}_l^H \boldsymbol{\Theta}_l \mathbf{G}_l + \mathbf{h}_{de}^H\right)\mathbf{w}\right\|^2}{\sigma_e^2}\right). \end{aligned} \tag{14}$$

To construct a more tractable surrogate function to approximate the original non-convex objective function, with $\bar{\mathbf{h}}_{u,l} = \operatorname{diag}\left(\mathbf{h}_l^H\right)\mathbf{G}_l$ and $\bar{\mathbf{h}}_{e,l} = \operatorname{diag}\left(\mathbf{g}_l^H\right)\mathbf{G}_l$ we introduce auxiliary variables $\gamma_{u,1}$, $\gamma_{u,2}$, $\gamma_{e,2}$, and $\gamma_{e,p}$ defined as

$$\gamma_{u,1} = \left\|\left(\sum_{l=1}^{L} \boldsymbol{\theta}_l^H \bar{\mathbf{h}}_{u,l} + \mathbf{h}_{du}^H\right)\mathbf{w}\right\|^2, \tag{15a}$$

$$\gamma_{u,2} = \left\|\left(\sum_{l=1}^{L} \boldsymbol{\theta}_l^H \bar{\mathbf{h}}_{u,l} + \mathbf{h}_{du}^H\right)\mathbf{w}\right\|^2 + \sigma^2, \tag{15b}$$

$$\gamma_{e,2} = 1 + \frac{\left\|\left(\sum_{l=1}^{L} \boldsymbol{\theta}_l^H \bar{\mathbf{h}}_{e,l} + \mathbf{h}_{de}^H\right)\mathbf{w}\right\|^2}{\sigma_e^2}, \tag{15c}$$

$$\gamma_{e,p} = 1 + \frac{\left\|\sum_{l=1}^{L} \boldsymbol{\theta}_l^H \bar{\mathbf{h}}_{e,l} + \mathbf{h}_{de}^H\right\|_F^2 P}{\sigma_e^2}. \tag{15d}$$

Next, by taking advantage of the Lagrangian dual transform technique as [58], R_U can be reformulated by

$$R_U = \log(1 + a_1) - a_1 + (1 + a_1)\frac{\gamma_{u,1}}{\gamma_{u,2}}, \tag{16}$$

where a_1 is the auxiliary variable introduced by the transformation. We note that R_E contains a negative logarithm function and is thus difficult to solve directly via the Lagrangian dual transformation. Then, we introduce the auxiliary variables $\gamma_{e,p}$ and $\gamma_{e,2}$ to construct an equivalent expression of R_E, which is given by

$$R_E = \log\left(1 + \frac{\gamma_{e,p} - \gamma_{e,2}}{\gamma_{e,2}}\right) - \log(\gamma_{e,p}). \tag{17}$$

From the Cauchy-Schwarz inequality, it holds $\gamma_{e,2} = \left\|\left(\sum_{l=1}^{L} \boldsymbol{\theta}_l^H \bar{\mathbf{h}}_{e,l} + \mathbf{h}_{de}^H\right)\mathbf{w}\right\|^2 \le \left(\left\|\sum_{l=1}^{L} \boldsymbol{\theta}_l^H \bar{\mathbf{h}}_{e,l} + \mathbf{h}_{de}^H\right\|_F^2 \|\mathbf{w}\|^2\right) \le \left(\left\|\sum_{l=1}^{L} \boldsymbol{\theta}_l^H \bar{\mathbf{h}}_{e,l} + \mathbf{h}_{de}^H\right\|_F^2 P\right) = \gamma_{e,p}$, and thus the fractional terms in logarithm is non-negative. Then, by applying the Lagrangian dual transform technique again, R_E can be rewritten in the following form

$$R_E = \log(1 + a_2) - a_2 + (1 + a_2)\frac{\gamma_{e,p} - \gamma_{e,2}}{\gamma_{e,p}} - \log(\gamma_{e,p}), \tag{18}$$

where a_2 is the auxiliary variable. Noting that the objective is still non-convex, we transform the original objective into the problem (P1.1) based on the idea of decoupled optimization of numerators and denominators in the quadratic transform technique [58].

$$\begin{aligned} (\text{P1.1}) \quad & \max_{\mathbf{w},\boldsymbol{\theta},\mathrm{a}_1,\mathrm{a}_2,\rho} \tilde{\mathrm{R}}_{\mathrm{s}} = \log(1 + \mathrm{a}_1) + \log(1 + \mathrm{a}_2) \\ & - \log(1 + \frac{\left\|\sum_{l=1}^{L} \boldsymbol{\theta}_l^H \bar{\mathbf{h}}_{e,l} + \mathbf{h}_{de}^H\right\|_F^2 P}{\sigma_e^2}) \\ & + 2\rho\sqrt{(1 + a_1)}\Re\left\{\left(\sum_{l=1}^{L} \boldsymbol{\theta}_l^H \bar{\mathbf{h}}_{u,l} + \mathbf{h}_{du}^H\right)\mathbf{w}\right\} \\ & - \rho^2\left(\left\|\left(\sum_{l=1}^{L} \boldsymbol{\theta}_l^H \bar{\mathbf{h}}_{u,l} + \mathbf{h}_{du}^H\right)\mathbf{w}\right\|^2 + \sigma^2\right) - (a_1 + a_2) + (1 + a_2) \\ & \times \frac{\left\|\sum_{l=1}^{L} \boldsymbol{\theta}_l^H \bar{\mathbf{h}}_{e,l} + \mathbf{h}_{de}^H\right\|_F^2 P - \left\|\left(\sum_{l=1}^{L} \boldsymbol{\theta}_l^H \bar{\mathbf{h}}_{e,l} + \mathbf{h}_{de}^H\right)\mathbf{w}\right\|^2}{\sigma_e^2 + \left\|\sum_{l=1}^{L} \boldsymbol{\theta}_l^H \bar{\mathbf{h}}_{e,l} + \mathbf{h}_{de}^H\right\|_F^2 P}, \\ & \text{s.t.} \qquad (12b), (12c), \end{aligned} \tag{19}$$

where ρ is the new auxiliary introduced by transformation.

3.2 Active Beamforming Design

We fix the passive beamforming variable $\boldsymbol{\theta}$. Note that $\tilde{R}_s$ is convex with the $\mathbf{w}$, a_1, a_2, ρ when other variables are fixed. Hence, we can employ the block coordinate descent method [59] to attain the optimal values of a_1, a_2 and ρ by setting the derivative to zero, while keeping other variables fixed. The closed-form solution for updating the variable a_1, a_2 and ρ at the t-th iteration can be given by

$$a_1^{(t)} = \left(\sqrt{1 + \frac{4}{\vartheta_1^{(t-1)}}} + 1\right)\frac{\vartheta_1^{(t-1)}}{2}, \tag{20a}$$

$$a_2^{(t)} = \frac{\gamma_{e,p}^{(t-1)} - \gamma_{e,2}^{(t-1)}}{\gamma_{e,2}^{(t-1)}}, \tag{20b}$$

$$\rho^{(t)} = \frac{\sqrt{1 + a_1^{(t-1)}}\Re\left\{\vartheta_2^{(t-1)}\right\}}{\gamma_{u,2}^{(t-1)}}, \tag{20c}$$

where $\vartheta_1 = \rho^2\gamma_{u,1}$ and $\vartheta_2 = \left(\sum_{l=1}^{L} \boldsymbol{\theta}_l^H \bar{\mathbf{h}}_{u,l} + \mathbf{h}_{du}^H\right)\mathbf{w}$. For the variable $\mathbf{w}$, the dual variable $\hat{\lambda}$ is introduced to deal with the power constraint. When other variables are given, by constructing a Lagrangian function of the objective function in the problem (P1.1), the closed-form solution to the active beamforming subproblem is

$$\begin{aligned} \mathbf{w}^{(t)} = {} & \sqrt{1 + a_1^{(t-1)}}\Re\left\{\sum_{l=1}^{L} \bar{\mathbf{b}}_{u,l}^{(t-1)} + \mathbf{h}_{du}\right\}\Bigg[\left(\rho^{(t-1)}\right)^2 \bar{\mathbf{B}}_u^{(t-1)} \\ & + \left(1 + a_2^{(t-1)}\right)\frac{\bar{\mathbf{B}}_e^{(t-1)}}{\left\|\sum_{l=1}^{L} \bar{\mathbf{b}}_{e,l}^{(t-1)} + \mathbf{h}_{de}\right\|_F^2 P + \sigma_e^2} + \hat{\lambda}\mathbf{I}_N\Bigg]^{-1}\rho^{(t-1)}, \end{aligned} \tag{21}$$

where $\bar{\mathbf{B}}_u = \sum_{l=1}^{L} \bar{\mathbf{b}}_{u,l}^H \bar{\mathbf{b}}_{u,l} + \sum_{l=2}^{L}\sum_{i=1}^{l-1} \bar{\mathbf{b}}_{u,l}^H \bar{\mathbf{b}}_{u,i} + 2\mathbf{h}_{du}\bar{\mathbf{b}}_{u,l} +$

$\mathbf{h}_{du}\mathbf{h}_{du}^H$, $\bar{\mathbf{B}}_e = \sum_{l=1}^{L} \bar{\mathbf{b}}_{e,l}^H \bar{\mathbf{b}}_{e,l} + \sum_{l=2}^{L}\sum_{i=1}^{l-1} \bar{\mathbf{b}}_{e,l}^H \bar{\mathbf{b}}_{e,i} + 2\mathbf{h}_{de}\bar{\mathbf{b}}_{e,l} + \mathbf{h}_{de}\mathbf{h}_{de}^H$, $\bar{\mathbf{b}}_{u,l} = \sum_{l=1}^{L} \boldsymbol{\theta}_l^H \bar{\mathbf{h}}_{u,l}$ and $\bar{\mathbf{b}}_{e,l} = \boldsymbol{\theta}_l^H \bar{\mathbf{h}}_{e,l}$. To obtain the optimal value of the Lagrangian multiplier, the binary search method is a possible solution which, however, could greatly increase the complexity. Thus, inspired by [43], we use the prox-linear BCD updating technique to reduce the iteration times for searching $\hat{\lambda}$.

Note that the block for $\mathbf{w}$ is a convex problem while all other blocks are fixed at their last updated values, which satisfies the constraint required for convergence in the prox-linear BCD updates [60]. Then, we attain the optimal solution of $\mathbf{w}$ at each iteration by updating

$$\begin{aligned}\mathbf{w}^{(t+1)} =& \arg\min_{\mathbf{w}}\Big(\langle -\nabla\tilde{R}_s(\tilde{\mathbf{w}}^{(t)}), \mathbf{w}-\tilde{\mathbf{w}}^{(t)}\rangle \\ &+ \frac{C^t}{2}\left\|\mathbf{w}-\tilde{\mathbf{w}}^{(t)}\right\|^2\Big), \\ &\text{s.t.} \quad (12b),\end{aligned} \tag{22}$$

where the Lipschitz constant of the block-partial gradient is expressed as

$$C = \left\|\left(2\rho^2\bar{\mathbf{B}}_u + 2(1+a_2)\frac{\bar{\mathbf{B}}_e}{\left\|\sum_{l=1}^{L}\bar{\mathbf{b}}_{e,l}+\mathbf{h}_{de}\right\|_F^2 P+\sigma_e^2}\right)\right\|_F. \tag{23}$$

The extrapolated point $\tilde{\mathbf{w}}^{(t)} = \mathbf{w}^{(t)} + \varsigma\left(\mathbf{w}^{(t)} - \mathbf{w}^{(t-1)}\right)$, where the extrapolation weight $\varsigma^{(t)} = \min(\hat{\varsigma}^{(t)}, \delta\sqrt{(C^{(t-1)})/C^{(t)}})$ satisfies $\delta < 1$ and $\hat{\varsigma}^t = \left(e^{(t-1)}-1\right)/e^{(t)}$ with $e^0 = 1$, and $e^{(t)} = (1+\sqrt{1+4(e^{(t-1)})^2})/2$. From (19), the block-partial gradient at $\tilde{\mathbf{w}}^{(t)}$ can be obtained as

$$\begin{aligned}\nabla\tilde{R}_s(\tilde{\mathbf{w}}^{(t)}) =& 2\rho\sqrt{1+a_1}\Re\left\{\sum_{l=1}^{L}\bar{\mathbf{b}}_{u,l}+\mathbf{h}_{du}\right\} - 2\rho^2\bar{\mathbf{B}}_u\tilde{\mathbf{w}}^{(t)} \\ &- 2(1+a_2)\left(\frac{\bar{\mathbf{B}}_e\tilde{\mathbf{w}}^{(t)}}{\left\|\sum_{l=1}^{L}\bar{\mathbf{b}}_{e,l}+\mathbf{h}_{de}\right\|_F^2 P+\sigma_e^2}\right).\end{aligned} \tag{24}$$

Since the problem (P1.1) is convex with respect to $\mathbf{w}$, based on the Lagrange multiplier method, the optimal active beamforming solution can be obtained

$$\mathbf{w}^{(t+1)} = \frac{1}{C^{(t)}-2\hat{\lambda}}\left(C^{(t)}\tilde{\mathbf{w}}^{(t)} + \nabla\tilde{R}_s(\tilde{\mathbf{w}}^{(t)})\right), \tag{25}$$

where the Lagrange multiplier for the power constraint (12b) can be updated by

$$\hat{\lambda}^* = \frac{C^{(t)}}{2} - \frac{\left\|C^{(t)}\tilde{\mathbf{w}}^{(t)} + \nabla R_s(\tilde{\mathbf{w}}^{(t)})\right\|^2}{2P}. \tag{26}$$

By reducing the iteration times for searching λ, and utilizing a more efficient technique than the original BCD technique as proved in [60], the complexity of the algorithm for active beamforming optimization can be greatly reduced, which will be further discussed in Sect. 5.

3.3 Passive Beamforming Design

After updating the value of $\mathbf{w}$ according to (25), we aim to optimize the passive beamforming variable $\boldsymbol{\theta}$. Unfortunately, the subproblem of passive beamforming optimization is non-convex and more difficult than directly optimizing the active beamforming due to the unit-modulus constraint. To address this difficulty, we first reformulate the expressions of the objective function R_S in terms of $\boldsymbol{\theta}$ by constructing $\hat{\boldsymbol{\Theta}} = [\boldsymbol{\theta}_1, \cdots, \boldsymbol{\theta}_L]$, $\mathbf{V}_i = [\mathbf{v}_{i,1}, \mathbf{v}_{i,2}, \cdots, \mathbf{v}_{i,L}]$, $i \in \{u, e\}$, where $\mathbf{v}_{u,l} = \mathrm{diag}(\mathbf{h}_l^H)\mathbf{G}_l\mathbf{w}$, $\mathbf{v}_{e,l} = \mathrm{diag}(\mathbf{g}_l^H)\mathbf{G}_l\mathbf{w}$. We also denote $\hat{\boldsymbol{\theta}} = \mathrm{vec}(\hat{\boldsymbol{\Theta}})$, $\mathbf{v}_i = \mathrm{vec}(\mathbf{V}_i)$, and

$$\bar{\gamma}_{u,1} = \left\|\mathbf{h}_{du}^H\mathbf{w} + \hat{\boldsymbol{\theta}}^H\mathbf{v}_u\right\|^2, \tag{27a}$$

$$\bar{\gamma}_{u,2} = \left\|\mathbf{h}_{du}^H\mathbf{w} + \hat{\boldsymbol{\theta}}^H\mathbf{v}_u\right\|^2 + \sigma^2, \tag{27b}$$

$$\bar{\gamma}_{e,2} = 1 + \frac{\left\|\mathbf{h}_{de}^H\mathbf{w} + \hat{\boldsymbol{\theta}}^H\mathbf{v}_e\right\|^2}{\sigma_e^2}, \tag{27c}$$

$$\bar{\gamma}_{e,1} = 1 + \frac{\left(\left\|\mathbf{h}_{de}^H\mathbf{w}\right\| + \sqrt{M}\left\|\mathrm{tr}(\mathbf{V}_e)\right\|\right)^2}{\sigma_e^2}. \tag{27d}$$

Then, R_U in (14) is equivalent to

$$R_U = \log(1+a_1) + (1+a_1)\frac{\bar{\gamma}_{u,1}}{\bar{\gamma}_{u,2}} - a_1. \tag{28}$$

Based on the triangle inequality and the constraint (12c), we can obtain $\|\mathbf{h}_{de}^H\mathbf{w} + \hat{\boldsymbol{\theta}}^H\mathbf{v}_e\|^2 \le (\left\|\mathbf{h}_{de}^H\mathbf{w}\right\| + \|\hat{\boldsymbol{\theta}}^H\mathbf{v}_e\|)^2 \le (\left\|\mathbf{h}_{de}^H\mathbf{w}\right\| + \sqrt{M}\left\|\mathrm{tr}(\mathbf{V}_e)\right\|)^2$, which shows that the function $(\bar{\gamma}_{e,1} - \bar{\gamma}_{e,2})$ is non-negative. Again, by constructing an equivalent expression to R_E and applying the Lagrangian dual transform technique, we can obtain

$$\begin{aligned}R_E =& \log(1+a_2) - \log(\bar{\gamma}_{e,1}) \\ &+ (1+a_2)\left(\frac{\bar{\gamma}_{e,1}-\bar{\gamma}_{e,2}}{\bar{\gamma}_{e,1}}\right) - a_2.\end{aligned} \tag{29}$$

After dropping the constant terms and applying the quadratic transform technique, the original optimization problem can be reformulated into (P1.2), where $D_i = \mathbf{h}_{di}^H\mathbf{w}, i \in \{u, e\}$.

$$\begin{aligned}(\text{P1.2}) \quad &\max_{\boldsymbol{\theta}, \mathrm{a}_1, \mathrm{a}_2, \hat{\rho}} \hat{\mathrm{R}}_\mathrm{s} = 2\hat{\rho}\sqrt{(1+a_1)}\Re\left\{\mathrm{D_u} + \hat{\boldsymbol{\theta}}^\mathrm{H}\mathbf{v}_\mathrm{u}\right\} \\ &- \hat{\rho}^2\left(\left\|D_u + \hat{\boldsymbol{\theta}}^H\mathbf{v}_u\right\|^2 + \sigma^2\right) \\ &+ (1+a_2)\left(\frac{(\|D_e\| + \sqrt{M}\left\|\mathrm{tr}(\mathbf{V}_e)\right\|)^2 - \left\|D_e + \hat{\boldsymbol{\theta}}^H\mathbf{v}_e\right\|^2}{\sigma_e^2 + (\|D_e\| + \sqrt{M}\left\|\mathrm{tr}(\mathbf{V}_e)\right\|)^2}\right), \\ &\text{s.t.} \qquad (12c).\end{aligned} \tag{30}$$

Note that problem (P1.2) is convex with the auxiliary variable when other variables are fixed. Hence, the auxiliary

variables introduced by transformation techniques at the t-th iteration are given by

$$\hat{\rho}^{(t)} = \frac{\sqrt{(1+a_1^{(t-1)})}\Re\left\{D_u^{(t-1)} + \left(\hat{\boldsymbol{\theta}}^{(t-1)}\right)^H \mathbf{v}_u^{(t-1)}\right\}}{\|D_u^{(t-1)} + (\hat{\boldsymbol{\theta}}^{(t-1)})^H \mathbf{v}_u^{(t-1)}\|^2 + \sigma^2}. \tag{31}$$

It can be found that the problem (P1.2) is non-convex with respect to $\boldsymbol{\theta}$ when fixing all other variables, because of the unit-modulus constraints. To handle this problem, we let the phase shift as a substitute for $\theta_{m,l} = e^{j\phi_{m,l}}$, and construct $\hat{\boldsymbol{\Phi}} = [\boldsymbol{\phi}_1, \cdots, \boldsymbol{\phi}_l, \cdots, \boldsymbol{\phi}_L]$, where $\boldsymbol{\phi}_l = [\phi_{1,l}, \cdots, \phi_{M,l}]^T$. Then, the objective function can be transformed into a quadric form by letting

$$\mathbf{U} = \hat{\rho}^2 \mathbf{v}_u \mathbf{v}_u^H + (1+a_2)\frac{\mathbf{v}_e \mathbf{v}_e^H}{\sigma_e^2 + (\|D_e\| + \sqrt{M}\,\|\mathrm{tr}(\mathbf{V}_e)\|)^2}, \tag{32}$$

$$\mathbf{z} = \hat{\rho}\sqrt{(1+a_1)}\Re\{\mathbf{v}_u\} - \hat{\rho}^2 (D_u \mathbf{v}_u) - (1+a_2)\frac{D_e \mathbf{v}_e}{\sigma_e^2 + (\|D_e\| + \sqrt{M}\,\|\mathrm{tr}(\mathbf{V}_e)\|)^2}. \tag{33}$$

Therefore, the passive beamforming optimization subproblem can be reformulated as

$$\text{(P1.3)} \quad \min_{\hat{\boldsymbol{\phi}}} \quad \left[\left(\mathrm{e}^{\mathrm{j}\hat{\boldsymbol{\phi}}}\right)^{\mathrm{H}} \mathbf{U} \mathrm{e}^{\mathrm{j}\hat{\boldsymbol{\phi}}} - 2\Re\left\{(\mathrm{e}^{\mathrm{j}\hat{\boldsymbol{\phi}}})^{\mathrm{H}} \mathbf{z}\right\}\right], \tag{34}$$

where $\hat{\boldsymbol{\phi}} = \mathrm{vec}(\hat{\boldsymbol{\Phi}})$. To solve the non-convex problem in (34), we apply an inexact BCD method called the block successive convex approximation (BSCA) method [61] to guarantee convergence. Following the updating rule, we construct a convex second-order approximation of the objective function $\hat{R}_s$ at $\hat{\boldsymbol{\phi}}^{(t)}$ as the surrogate function, which is expressed as

$$\hat{R}_s(\hat{\boldsymbol{\phi}}|\hat{\boldsymbol{\phi}}^{(t)}) = \hat{R}_s\left(\hat{\boldsymbol{\phi}}^{(t)}\right) + \nabla\hat{R}_s\left(\hat{\boldsymbol{\phi}}^{(t)}\right)\left(\hat{\boldsymbol{\phi}} - \hat{\boldsymbol{\phi}}^{(t)}\right) + \frac{1}{2\tau}\left\|\hat{\boldsymbol{\phi}} - \hat{\boldsymbol{\phi}}^{(t)}\right\|^2. \tag{35}$$

Since the surrogate function (35) is a local approximation of the original function (34), to search for an optimal value with sufficient decrease, we adopt the line search with the Armijo step size selection rule, where the step size τ is the largest element in $\{\tau^0\beta^r\}_{r=0,1,\cdots}$, $\tau^0 > 0$, $\beta \in (0,1)$, satisfying

$$\hat{R}_s\left(\hat{\boldsymbol{\phi}}^{(t)}\right) - \hat{R}_s(\hat{\boldsymbol{\phi}}) \geq -\varepsilon\tau\left\|\nabla\hat{R}_s\left(\hat{\boldsymbol{\phi}}^{(t)}\right)\right\|^2, \tag{36}$$

where $\varepsilon \in (0,1)$, and the gradient with respect to $\hat{\boldsymbol{\phi}}$ is given by

$$\nabla\hat{R}_s(\hat{\boldsymbol{\phi}}) = 2\Re\left\{-je^{-j\hat{\boldsymbol{\phi}}}\left(\mathbf{U}e^{j\hat{\boldsymbol{\phi}}} - \mathbf{z}\right)\right\}. \tag{37}$$

Based on the minimum value of the surrogate function in (35), the gradient projection updating for the optimization variable $\boldsymbol{\phi}$ is quadratic programming with a closed-form solution

$$\hat{\boldsymbol{\phi}}^{(t)} = \hat{\boldsymbol{\phi}}^{(t-1)} - \tau\nabla\hat{R}_s. \tag{38}$$

With the function (34) continuously differentiable, τ can be properly chosen to make the surrogate function satisfy the following constraint

$$\hat{R}_s\left(\hat{\boldsymbol{\phi}}|\hat{\boldsymbol{\phi}}^{(t)}\right) \geq \hat{R}_s(\hat{\boldsymbol{\phi}}), \tag{39}$$

which guarantees the convergence of the algorithm based on the proposition in [61]. The equality can be obtained, when $\hat{\boldsymbol{\phi}} = \hat{\boldsymbol{\phi}}^{(t)}$.

The LCFP algorithm also can be easily extended to a RIS-aided SR maximization optimization problem associated with CSI errors, since the coordinated optimization algorithms for subproblems satisfy the convergence conditions to solve a two-level stochastic non-convex optimization problem [62]. Therefore, considering reducing the complexity and the cost of obtaining CSI, we extend the LCFP algorithm to a more practical scenario in the next section.

4. The LCRFP Algorithm for Secrecy Rate Optimization with Imperfect CSI

In this section, we investigate the SR maximization problem under a more practical scenario where both the CSI of Bob and Eve are imperfect.

4.1 Active Beamforming Design at the First Level

As analyzed in Sect. 2, problem (P2) is a two-level stochastic non-convex optimization problem containing expectation operators with respect to the random system state, which is more difficult to solve compared with (P1). To address this challenging problem, we propose a robust and low-complexity PLS enhancement algorithm based on the statistical CSI error model to maximize the SR. Our method can reduce the impact of the CSI mismatch by combining the benefits of the stochastic non-convex optimization techniques [62] and the LCFP algorithm, which is referred to as the LCRFP algorithm, as presented in Algorithm 2. This algorithm consists of three major steps. First, based on the problem transformation technique in the LCFP algorithm, the problem (P2) is decoupled into two subproblems, which can be optimized at different levels. Next, in the case of given $\bar{\boldsymbol{\theta}}$, we have the first-level subproblem with respect to $\mathbf{w}(\delta)$, which is the first-level optimization variable under the system state. To deal with the random system state and satisfy the assumptions when employing the stochastic successive convex approximation techniques [62], we initially transform the objective into a minimization problem. Then, following a similar approach used in the LCFP algorithm (Sect. 3.1) for active beamforming design, we employ the FP transformation technique to address logarithmic and fractional components by introducing auxiliary variables $\bar{a}_1$, $\bar{a}_2$ and $\bar{\rho}$. The first-level optimization subproblem can be reformulated as

Algorithm 2 The LCRFP Algorithm for Imperfect CSI.

Input: $\{\varrho^{(t)}\}$, initialize $t = 0$, $\mathbf{w}(\delta)^0$, δ^0, $\boldsymbol{\theta}^0$, and τ^0.
  repeat
    Set $t = t + 1$, and realize the channel about $\delta^{(t)}$;
    Solve the first-level subproblem (P1.1) to obtain the optimal solution $\mathbf{w}(\delta)^{(t)}$ with the given $\delta^{(t)}$ and auxiliary variables;
    Construct $\hat{\boldsymbol{\theta}}^{(t)}$, $\mathbf{v}_u$ and $\mathbf{v}_e$ based on given $\mathbf{w}(\delta)^{(t)}$ and $\boldsymbol{\theta}^{(t-1)}$;
    Transform $\hat{\boldsymbol{\theta}}^{(t)}$ to $\hat{\boldsymbol{\phi}}^{(t)}$;
    Update the $\mathbf{U}, \mathbf{z}$ based on the solution of the first-level subproblem $\mathbf{w}(\delta)^{(t)}$ and $\delta^{(t)}$;
    Calculate the $\nabla_{\hat{\boldsymbol{\phi}}} k\left(\hat{\boldsymbol{\phi}}, \mathbf{w}(\delta); \delta\right)$ by (45);
    Update the gradient $\mathbf{k}_{\hat{\boldsymbol{\phi}}}^{(t)}$ by (44) based on the solution of $\nabla_{\hat{\boldsymbol{\phi}}} k\left(\hat{\boldsymbol{\phi}}, \mathbf{w}(\delta); \delta\right)$;
    Design τ using Armijo rule according to $\hat{\boldsymbol{\phi}}^{(t)}$, $\mathbf{w}(\delta)^{(t)}$;
    Update $\hat{\boldsymbol{\phi}}^{(t)}$ with (47), and transform $\hat{\boldsymbol{\phi}}^{(t)}$ to $\hat{\boldsymbol{\theta}}^{(t)}$;
    With given $\hat{\boldsymbol{\theta}}^{(t)}$, update $\boldsymbol{\theta}^{(t)}$;
  Until the stopping criterion is met.
Output: $\mathbf{w}, \boldsymbol{\theta}$.

$$\text{(P2.1)} \quad \min_{\mathbf{w}(\delta), \bar{a}_1, \bar{a}_2, \bar{\rho}} \; -\tilde{R}_s\left(\bar{\boldsymbol{\theta}}, \mathbf{w}(\delta), \bar{a}_1, \bar{a}_2, \bar{\rho}; \delta\right), \tag{40a}$$

$$\text{s.t.} \quad \operatorname{tr}\left(\mathbf{w}(\delta)\,\mathbf{w}(\delta)^H\right) \leqslant P, \quad \forall \delta, \tag{40b}$$

where $\tilde{R}_s$ is the same form as in (P1.1). As problem (P2.1) is convex with the $\bar{a}_1, \bar{a}_2, \bar{\rho}$ when other variables are fixed, we can obtain a similar closed-form solution of auxiliary variables $\bar{a}_1$, $\bar{a}_2$ and $\bar{\rho}$ as in (20a) (20b) (20c). To derive a closed-form solution to $\mathbf{w}(\delta)$, we first construct a Lagrangian function of the objective to deal with the power constraint. Then, by employing the prox-linear BCD updating technique, which is the same as Algorithm 1 and omitted for simplicity, we obtain the optimal active beamforming solution as depicted in (25). Therefore, during the t-th iteration, after realizing the channel about $\delta(t)$, the auxiliary variables and the optimal solution $\mathbf{w}(\delta)$ can be updated, respectively.

To obtain a stationary solution for the first-level subproblem, we analyze the convergence of the algorithm devised for handling this subproblem. It has been established in [62] that the algorithm design must adhere to three conditions to guarantee convergence. The first condition is met by properly selecting the initial point. Subsequently, the updating equation for each variable within $\mathbf{w}(\delta), a_1, a_2$ exhibits Lipschitz continuity when the other two variables are held constant, satisfying the second convergence criterion. Lastly, we fulfill the third convergence requirement by leveraging the verified global convergence of the prox-linear block coordinate method as outlined in [60]. Therefore, by adhering to these conditions, the optimization algorithm for the first-level subproblem is capable of converging, leading to the stationary solution $\mathbf{w}(\delta)^*$.

4.2 Passive Beamforming Design at the Second Level

After obtaining the corresponding first-level variable $\mathbf{w}(\delta)^{(t)}$ with respect to a new realization of the channel realizations about $\delta^{(t)}$ by running the first-level algorithm in the t-th iteration, we have the second-level subproblem (P2.2) as followed

$$\text{(P2.2)} \quad \min_{\hat{\boldsymbol{\phi}}} \quad k(\hat{\boldsymbol{\phi}}) = \mathbb{E}_{\delta}\left[-\tilde{R}_s\left(\hat{\boldsymbol{\phi}}, \mathbf{w}(\delta); \delta\right)\right], \tag{41}$$

where $\hat{\boldsymbol{\phi}}$ is the second-level optimization variable, which is a substitute for $\hat{\boldsymbol{\theta}}^{(t)}$ to deal with the non-convex constraint, which is constructed in the method of Sect. 3.3. As in the passive beamforming design of the LCFP algorithm, the surrogate function $\bar{k}(\hat{\boldsymbol{\phi}})$ is designed as a convex approximation of the objective function of the problem (P2.2). Therefore, the optimal solution $\hat{\boldsymbol{\phi}}^{(t)}$ is solved as

$$\hat{\boldsymbol{\phi}}^{(t)} = \arg\min_{\hat{\boldsymbol{\phi}}} \quad \bar{k}^{(t)}(\hat{\boldsymbol{\phi}}), \tag{42}$$

To obtain a stationary solution to the second-level subproblem, we first design a convex surrogate function $\bar{k}(\hat{\boldsymbol{\phi}})$ based on the method in (35) of the LCFP algorithm, and this surrogate function satisfy the assumptions of the stochastic non-convex optimization to ensure the convergence of the algorithm, as shown in (39). The approximation of the objective function is expressed as

$$\bar{k}^{(t)}(\hat{\boldsymbol{\phi}}) = k(\hat{\boldsymbol{\phi}})^{(t)} + \mathbf{k}_{\hat{\boldsymbol{\phi}}}^{(t)}\left(\hat{\boldsymbol{\phi}} - \hat{\boldsymbol{\phi}}^{(t)}\right) + \tau\left\|\hat{\boldsymbol{\phi}} - \hat{\boldsymbol{\phi}}^{(t)}\right\|^2. \tag{43}$$

Then, we construct the recursive approximation of the second-level subproblem to adapt to the properties of the first-level subproblem solution with the help of the key theorem for surrogate function design in the stochastic non-convex optimization [62]. Therefore, with the initial value $\mathbf{k}_{\hat{\boldsymbol{\phi}}}^{-1} = 0$, the approximation of the partial derivative $\nabla_{\hat{\boldsymbol{\phi}}} k\left(\hat{\boldsymbol{\phi}}, \mathbf{w}(\delta); \delta\right)$, $\mathbf{k}_{\hat{\boldsymbol{\phi}}}$ in (43) updates recursively as

$$\mathbf{k}_{\hat{\boldsymbol{\phi}}}^{(t)} = (1 - \varrho^{(t)})\mathbf{k}_{\hat{\boldsymbol{\phi}}}^{(t-1)} + \varrho^{(t)} \nabla_{\hat{\boldsymbol{\phi}}} k\left(\hat{\boldsymbol{\phi}}^{(t)}, \mathbf{w}(\delta)^{(t)}; \delta^{(t)}\right), \tag{44}$$

where $\varrho^{(t)} \in (0, 1]$ is a sequence satisfying $\sum_t \varrho^{(t)} = \infty$, $\sum_t \left(\varrho^{(t)}\right)^2 < \infty$. And the gradient of $k(\hat{\boldsymbol{\phi}}, \mathbf{w}(\delta); \delta)$ with respect to $\hat{\boldsymbol{\phi}}$ in (44) is given by

$$\nabla_{\hat{\boldsymbol{\phi}}} k\left(\hat{\boldsymbol{\phi}}, \mathbf{w}(\delta); \delta\right) = 2\Re\left\{-je^{-j\hat{\boldsymbol{\phi}}}\left(\mathbf{U}e^{j\hat{\boldsymbol{\phi}}} - \mathbf{z}\right)\right\}. \tag{45}$$

As such, the constant $k(\hat{\boldsymbol{\phi}})^{(t)}$, with the initial value $k_{\hat{\boldsymbol{\phi}}}^{-1} = 0$, can be calculated via a recursive formula as

$$k(\hat{\boldsymbol{\phi}})^{(t)} = (1 - \varrho^{(t)})k(\hat{\boldsymbol{\phi}})^{(t-1)} + \varrho^{(t)} k\left(\hat{\boldsymbol{\phi}}^{(t)}, \mathbf{w}(\delta)^{(t)}; \delta^{(t)}\right). \tag{46}$$

With the expression of $\mathbf{U}$ and $\mathbf{z}$ already given in the previous section, the approximation of the problem (P2.2) is quadratic programming with respect to the passive beamforming variable $\hat{\boldsymbol{\phi}}$, which leads to a closed-form solution given by

$$\hat{\boldsymbol{\phi}}^{(t+1)} = \hat{\boldsymbol{\phi}}^{(t)} - \frac{\mathbf{k}_{\hat{\boldsymbol{\phi}}}^{(t)}}{2\tau}. \tag{47}$$

As described above, with the convergence conditions satisfied in each level of subproblem optimization, the LCRFP algorithm can obtain a stationary solution by solving the non-convex stochastic joint optimization problem (P2) under the impact of imperfect BCSI and ECSI in a RIS-aided mmWave system.

5. Complexity Analysis

In this section, we analyze the complexity of the proposed algorithms and compare them with some widely used methods for SR maximization in RIS-aided systems. First, in the LCFP algorithm, the complexity to update auxiliary variables and the active beamforming variable $\mathbf{w}$ is $O(2LMN + N^2)$, and the updating loop for this part is $I_{\mathbf{w}} = 1$, since the closed-form solutions can be obtained. The complexity of solving (32) and (33) in the passive beamforming optimization is at most $O(L^2M^2)$, and I_A is the updating loop for step searching due to applying the Armijo-type line search. Therefore, the entire complexity of the LCFP algorithm is $O(I_L(I_A(2MN + N^2) + (LM)^2))$, where I_L is the integral updating loop required for the optimization algorithm convergence. Then, we consider the complexity of the PLS enhancement algorithm based on other existing methods. In an SCA-based [42] PLS enhancement algorithm, the complexity of solving the passive beamforming subproblem is $O((LM)^{3.5})$. The MO method can address the unit-modulus constraint in the RIS-aided system, and the complexity of passive beamforming optimization based on the MO method [43] in the PLS enhancement algorithm is $O(I_{M,\boldsymbol{\theta}}L^2M^2)$. At the same time, the SCA technique is used to optimize the active beamforming as in [42]. We also analyze the complexity of the SDR-based [63] PLS enhancement algorithm. Table 1 summarizes the complexity comparison of the proposed algorithms and the aforementioned algorithms.

Evidently, the proposed algorithm has lower computation complexity than other algorithms. Since $N \ll M$, the main computational complexity of schemes lies in the passive beamforming optimization part. Therefore, the complexity of the SCA-based algorithm and the SDR-based algorithm is higher than the LCFP algorithm. Although the similar computational complexity in the passive beamforming optimization part $O((LM)^2)$, the active beamforming optimization part in the LCFP algorithm $O(N^2)$ still has a slightly higher complexity than the MO-based algorithm $O(N^3)$. The comparison shows that the proposed algorithm has lower computation complexity than benchmark algorithms. The complexity of the SCA-based algorithm and the SDR-based algorithm increases faster than the LCFP algorithm with the number of reflecting elements M increasing. Although there is similar computational complexity in the passive beamforming optimization part, the active beamforming optimization part in the LCFP algorithm $O(N^2)$ still has a slightly higher complexity than the MO-based algorithm $O(N^3)$. Moreover, with the variable $\mathbf{w}, \boldsymbol{\theta}$ coupled, the MO-based algorithm optimizes the subproblems independently, which is hard to extend to the imperfect CSI case. In summary, the LCFP algorithm has advantages in extending to some complex scenarios and low complexity, especially when M is relatively large, conforming to the practical communication system.

Table 1 Comparison of algorithm complexity.

Algorithm	Complexity
LCFP algorithm	$O(I_L(I_A(2LMN + N^2) + (LM)^2))$
SCA-based algorithm	$O(I_C(I_{C,\mathbf{w}}N^3 + I_{C,\boldsymbol{\theta}}(LM)^{3.5}))$
MO-based algorithm	$O(I_M(I_{M,\mathbf{w}}N^3 + I_{M,\boldsymbol{\theta}}(LM)^2))$
SDR-based algorithm	$O(I_D(I_{D,\mathbf{w}}N^{6.5} + I_{D,\boldsymbol{\theta}}(LM)^{6.5}))$

Next, we analyze the complexity of the LCRFP algorithm. Besides the advantage of the low complexity of each algorithm to optimize the active beamforming or passive beamforming at different levels due to the basis of the LCFP algorithm, the updating method utilized in this algorithm also brings benefits in reducing the complexity. Compared with other updating methods to solve a two-level stochastic optimization problem, i.e., batch alternating optimization algorithm, which needs to minimize a sample average approximation function as $k_{\mathrm{SAA}}^{(t)}(\boldsymbol{\phi}) \triangleq \sum_{r=1}^{t} k(\boldsymbol{\phi}, \mathbf{w}(\phi^{(t)}, \delta^r)^*, \delta^r)$, where t is the iteration times, the updating method we applied needs fewer iterations. Since it only needs to solve the first-level problem with respect to the current system state $\delta^{(t)}$, batch alternating optimization needs to solve t times associated with all the previous system states to obtain the average approximation. The total complexity of the LCRFP algorithm is $O(I_R(I_AI_f(2LMN + N^2) + (LM)^2))$, where I_f denotes the iterative numbers of the first-level optimization subproblem to find a stationary solution.

6. Numerical Results

In this section, we evaluate the effectiveness of our proposed algorithms via simulation to verify the utility of the PLS enhancement in a RIS-aided mmWave system when jointly considering the non-neglectable practical issues. The schematic system model for the simulated RIS-aided mmWave system is shown in Fig. 1, where both Bob and Eve are regular users of the system. Alice serves as the transmitter equipped with $N = 4$ antennas and is situated at (0 m, 0 m). The location of the legitimate receiver (Bob) is (D_1 m, 0 m). Eve moves along a circular path with a radius of R m around Bob. Here, R, the distance between Bob and Eve, is initially set as 8 m, and the receiving distance denoted by D_1 is predefined as 70 m. To enhance the communication secrecy between Alice and Bob, L RISs are deployed around Bob. The number of the reflecting elements on each RIS is initially set as $M = 50$. The amplitude reflection coefficient is set as $\eta = 1$ to maximize the reflection strength. Assuming the channel $\mathbf{h}_{d,k}$ follows Rayleigh fading and $\mathbf{G}$, $\mathbf{g}$, and $\mathbf{h}$ follow Rician fading as in [43]. In the cascade channels of Alice-to-RIS, RIS-to-Bob, and RIS-to-

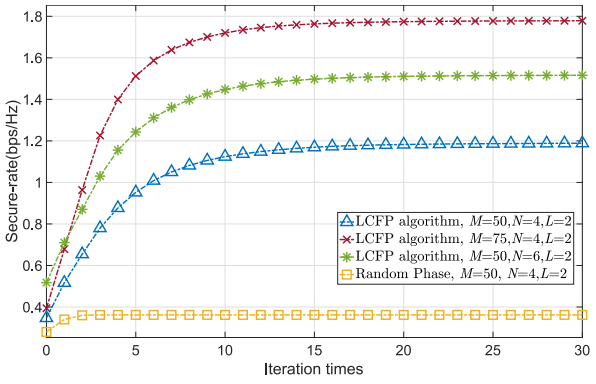

Fig. 2 Convergence of the LCPF algorithm versus different RIS size and transmit antennas.

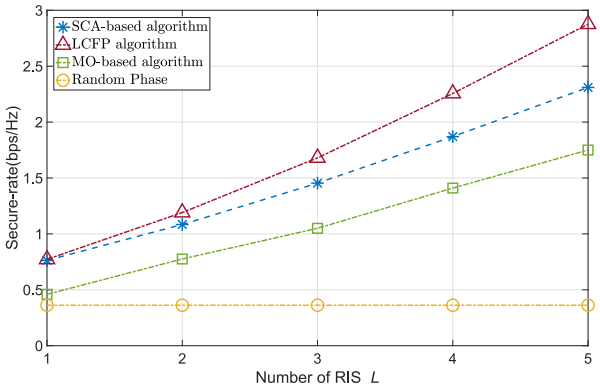

Fig. 3 The algorithms versus different RIS numbers.

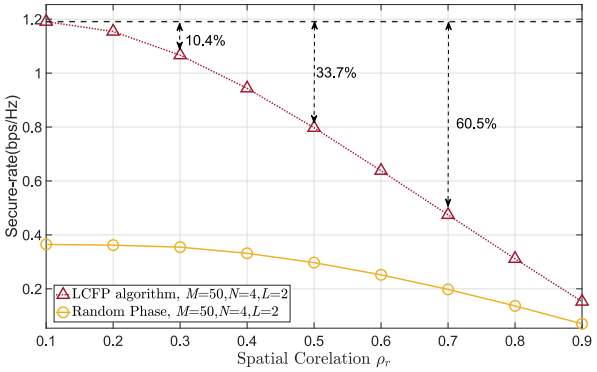

Fig. 4 The algorithms versus different spatial correlation.

Eve, the Rician factor is set as $\kappa = 10$. The path loss exponent of the RIS-related channels is set to 2.2, and that of the direct Alice-Bob and Alice-Eve channels is set to 3.67. The spatial correlation between Bob and Eve is initialized to a low level with $\rho = 0.1$. The total transmit power constraint is set to $P = 5$ dBm.

Firstly, we discuss the convergence behavior of the LCFP algorithm. As illustrated in Fig. 2, the proposed algorithm converges in the limit iterations by assuming the perfect CSI is obtained. Then, we set the random passive beamforming on RIS as a benchmark scheme. It can be seen that the SR of the random phase setting is very low (SR value is 0.36 bps/Hz) due to the more advantageous position of Eve. With a proper passive beamforming optimization of multiple distributed RISs, the proposed algorithm can achieve a secrecy performance gain that outperforms the random phase setting.

Secondly, we show the security performance of the LCFP algorithm versus different numbers of reflecting elements M and antennas N. It can be observed from Fig. 2 that the optimal SR increases with the number of reflecting elements or antennas increasing. Specially, by increasing the reflection number up to 50%, where $M = 75, N = 4$, the achievable SR increases by 49.6%. On the other hand, the achievable SR only increases by 27.5% when increasing the antenna number up to 50%, where $M = 50, N = 6$. Therefore, with the benefits of array gain, increasing the RIS size can provide a more obvious performance improvement than increasing the antenna number.

Next, we illustrate the variation of the achievable SR with the different number of RISs under different RIS-aided PLS enhancement schemes. By increasing the number of the RIS L from 1 to 5 with $P = 5$ dBm, $M = 50, N = 4$, we compare the secrecy performance achieved by the LCFP algorithm with the widely used SCA-based algorithm and MO-based algorithm mentioned in Sect. 5. The SDR-based algorithm is excluded from the simulation due to the high complexity, and the convergence is hard to be guaranteed. By setting the random passive beamforming RIS setting as the lower bound, we treat the MO-based [43] PLS enhancement algorithm and the SCA-based [42] PLS enhancement algorithm as benchmarks. Figure 3 shows that the achievable SR increases as the number of RISs increases under all the algorithms, except the random phase setting scheme. From the results, we can also obtain that the LCFP algorithm can achieve a better secrecy performance compared with the MO-based algorithm. In addition, with the RIS number increasing, the LCFP algorithm can achieve a better secrecy performance than the SCA-based algorithm. Therefore, the proposed LCFP algorithm outperforms the benchmarks in security performance.

Figure 4 evaluates the impact of spatial correlation between the eavesdropping and legitimate channels on security performance. By increasing the spatial correlation coefficient ρ_r from 0.1 (indicating a low level) to 0.9 (indicating a high level), with parameters set as $P = 5$ dBm, $M = 50$, and $N = 4$, we observe a decline in the achievable SR as the spatial correlation grows. Furthermore, this reduction in SR exhibits an amplified trend with increasing spatial correlation. Specifically, compared to a scenario with a low spatial correlation between Bob and Eve ($\rho_r = 0.1$), there is a 10.4% security performance loss as the spatial correlation escalates to 0.3. This reduction becomes more substantial, reaching 33.7%, as the spatial correlation is elevated to 0.5. Notably, an even more pronounced drop of 60.5% is observed with a spatial correlation of 0.7. This is attributed to the reduced channel capacity difference resulting from the decreased spatial correlation between le-

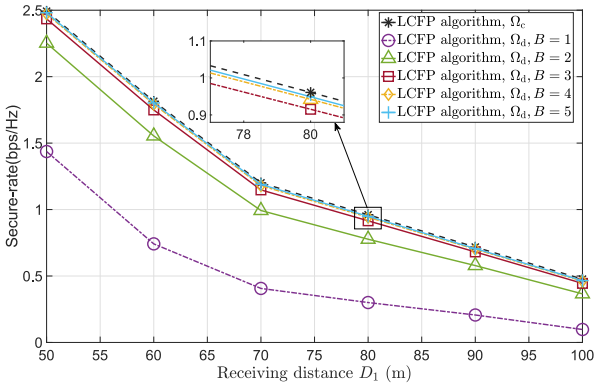

Fig. 5 The performance of proposed algorithm versus different resolution phase shifters.

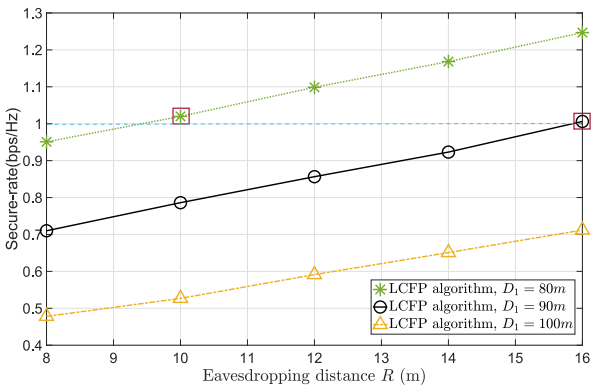

Fig. 6 The performance of proposed algorithm under different spatial positioning.

gitimate and eavesdropping users. However, the proposed LCFP algorithm outperforms the random phase scheme by optimizing the passive beamforming to deal with the performance loss caused by spatial correlation between the eavesdropping and legitimate channels.

Also, we study the impact of the different resolution phase shifters of the RIS on system secrecy performance. Herein, the infinite-resolution-continuous-phase shifter set is defined as $\mathbf{\Omega}_c$ for $\theta_{m,l}$, while the finite-resolution-discrete-phase shifter set as $\mathbf{\Omega}_d$, which are expressed as

$$\mathbf{\Omega}_c = \left\{\theta_{m,l} = e^{j\phi_{m,l}} | \phi_{m,l} \in [0, \cdots, 2\pi)\right\}, \tag{48}$$

$$\mathbf{\Omega}_d = \left\{\theta_{m,l} = e^{j\phi_{m,l}} | \phi_{m,l} = \frac{2\pi n}{2^B}, n \in [0, \cdots, 2^B - 1)\right\}, \tag{49}$$

where B is the number of quantization bits. As shown in Fig. 5, we exploit the secrecy rate gap between finite-resolution phase shifters and infinite-resolution phase shifters. The secrecy rate is plotted versus a range of distances D_1 from 50 m to 100 m between the transmitter (Alice) and receivers (Bob and Eve) with $M = 50, N = 4, L = 2$, and $R = 8$ m. As the phase shifter resolution B increases from 1 to 5, the secrecy rate gap in comparison to infinite-resolution phase shifters diminishes. Specially, at a distance $D_1 = 70$ m, this secrecy rate gap reduces from 0.21 bps/Hz to 0.02 bps/Hz when B varies from 2 to 4. Notably, this secrecy performance enhancement in finite-resolution phase shifters setting exhibits a diminishing trend once B exceeds a value of 3, suggesting a proper threshold for phase resolution. Figure 5 also indicates that increasing the distance D_1 has a detrimental effect on the secrecy performance. Nonetheless, when D_1 remains below a certain threshold, i.e., $D_1 \leq 77$ m, the system is capable of sustaining a secrecy rate above 1.0 bps/Hz, and this remains effective even when Bob and Eve are in a close distance of $R = 8$ m. Therefore, both spatial parameter D_1 and resolution B play pivotal roles in security performance, necessitating proper design based on practical scenarios. Building on the results of the diminishing returns observed beyond a certain resolution, a 3-bit setting appears as a practical choice, yielding near-optimal

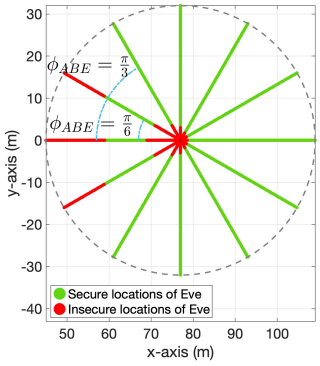

Fig. 7 The secure locations of Eve under different angles.

results compared to an infinite-resolution phase shifter setting.

Furthermore, we investigate the impact of the spatial parameters, including the eavesdropping distance between Eve and Bob R and the receiving distance D_1, on security performance. As delineated in Fig. 6, the secrecy rate increased with the extension of R or a decrease in D_1 attributable to the reduced correlation between legitimate and eavesdropping channels. This observation aligns with Fig. 4, establishing that enhanced spatial correlation reduces secrecy rates. Such an observed trend provides opportunities for maintaining secure transmissions even when distances D_1 exceed 77 m. For systematic analysis on secure locations of Eve, we set a fixed receiving distance $D_1 = 77$ m, and vary the location of Eve around a circle centered at Bob, utilizing predefined angles $\phi_{ABE} \in \{0, \frac{\pi}{6}, \frac{\pi}{3}, \frac{\pi}{2}, \frac{2\pi}{3}, \frac{5\pi}{6}, \pi, -\frac{5\pi}{6}, -\frac{2\pi}{3}, -\frac{\pi}{2}, -\frac{\pi}{3}, -\frac{\pi}{6}\}$. This configuration facilitates the systematic evaluation of the impact of eavesdropping distance (corresponding to the radius R of the circle) on the secrecy rate. With a threshold secrecy rate defined at 1.0 bps/Hz, we can obtain the secure locations of Eve. As illustrated in Fig. 7, the secure locations of Eve expand as ϕ_{ABE} increases from 0 to π, the angle relative to the line between Bob and Alice. Notably, when Eve is located between Bob and Alice ($\phi_{ABE} = 0$), a minimal secure location range of Eve is observed, confined between

(59 m, 0 m) and (69 m, 0 m). Two factors influence this behavior. First, as Eve moves away from Bob, the spatial correlation of the channels reduces, enhancing the secrecy rate. Then, as Eve moves closer to Alice while away from Bob, its eavesdropping capability increases, eventually offsetting the benefits garnered from spatial channel variations and reducing the secrecy rate below the threshold. In addition, the augmentation of ϕ_{ABE} can diminish the eavesdropping capability, thereby expanding the secure location range of Eve. For instance, when $\phi_{ABE} = \frac{\pi}{6}$, the secure locations of Eve lie between (59.6 m, 10 m) and (70.9 m, 3.5 m), a range nearly 13 m wider than the range at $\phi_{ABE} = 0°$. For angles in the domain $\frac{\pi}{2} \leq \phi_{ABE} \leq \pi$ and $-\frac{\pi}{2} \geq \phi_{ABE} \geq -\pi$, the secure eavesdropping range broadens, extending radially. Figure 7 also shows that the symmetrical nature of the observed trends for both positive ($0 \leq \phi_{ABE} \leq \pi$) and negative angles ($-\pi \leq \phi_{ABE} \leq 0$). Therefore, the spatial topological relationship between network nodes is essential for optimizing system security performance to construct secure transmission.

In addition, we evaluate the robustness of the LCRFP algorithm by comparing it with other benchmarks with channel mismatch. We assume that the statistical CSI error models of both Bob and Eve follow the CSCG distribution and set the relative amount of CSI uncertainty $\epsilon = \epsilon_G = \epsilon_h = \epsilon_g = \epsilon_{di}, i = \{u, e\}$ and $\epsilon = \{0.1, 0.3, 0.6\}$ to characterize the estimated precision, and the transmit power $P = 5$ dBm. Figure 8 compares the LCRFP algorithm with the non-robust algorithm (LCFP algorithm) in terms of secrecy rate versus the iteration number under the imperfect CSI ($\epsilon = 0.1$) setting. It shows that only the LCRFP algorithm achieves almost sure convergence to a solution after a few iterations, demonstrating the robustness of our proposed algorithm. Then, we depict the achievable SR versus different CSI uncertainty in Fig. 9. The non-robust algorithm under the perfect CSI setting is set as the upper bound, and the random phase scheme under the perfect CSI setting is set as the lower bound. It shows that increasing channel uncertainty ϵ leads to more iteration times to obtain the stationary solution by analyzing the achievable SR versus different CSI uncertainty. Furthermore, it can be seen that there has been an increasing secrecy performance loss with the CSI uncertainty increasing compared with the upper bound. However, the secrecy performance of our proposed algorithm is always over the lower bound. In particular, the proposed algorithm can increase up to 54.6% SR compared with the lower bound when CSI uncertainty is as low as 40%, demonstrating that the LCRFP method can mitigate the loss of the secrecy performance caused by the random system state. In addition, there is only 10.2% secrecy performance loss on the LCRFP algorithm when $\epsilon = 10\%$ (with a secrecy rate of 1.07 bps/Hz) compared with the upper bound. Therefore, we can achieve a close solution by the proposed algorithm with imperfect CSI to that in the case of perfect CSI when the estimation error is in a certain region, and the LCRFP algorithm can improve system secrecy performance compared with the non-robust benchmark schemes.

Finally, we delve into a more practical scenario characterized by imperfect CSI and finite-resolution phase shifters, offering a comprehensive understanding of how these factors impact secrecy performance. As presented in Fig. 10, we examine the impact of CSI uncertainty ($\epsilon \in \{0.1, 0.3, 0.6\}$) across various finite-resolution settings B. Compared with the infinite-resolution setting, we observe that secrecy performance loss amplifies as resolution B diminishes. Specifically, a marked decline is evident as resolution transitions from 1-bit to 3-bit, followed by a more

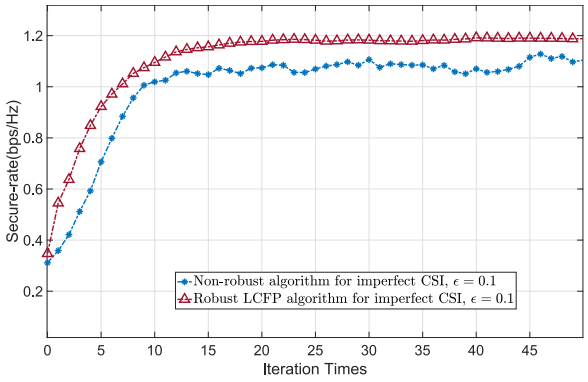

Fig. 8 Convergence of algorithms under imperfect CSI.

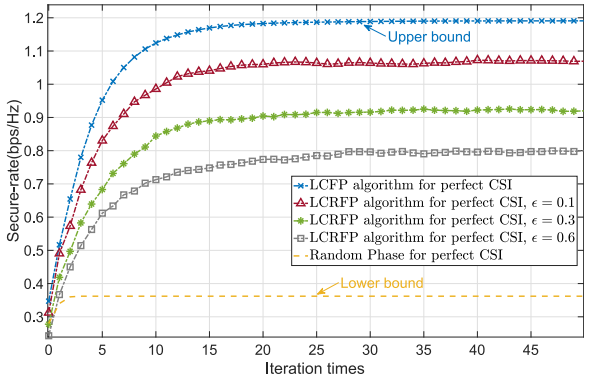

Fig. 9 The LCRPF algorithm versus different CSI uncertainty.

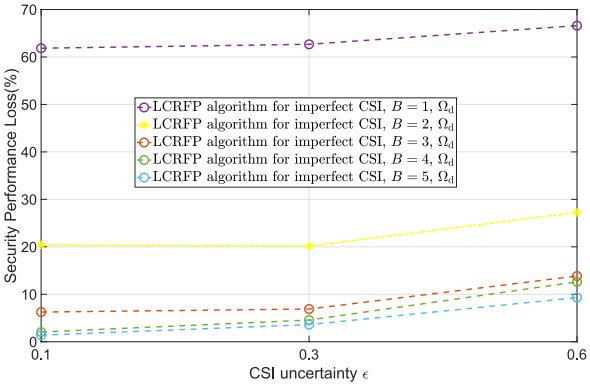

Fig. 10 The performance loss varies with CSI uncertainty under different finite resolution phase shifters compared with infinite resolution phase shifters.

modest reduction as the transition advances from 4-bit to 5-bit. Furthermore, as ϵ increases, the gradual increase in security performance loss becomes evident, which signifies that the SR achieved with a finite-resolution setting gradually falls behind the performance level of the infinite-resolution setting. This trend is attributed to the impact of quantization error, which degrades performance as CSI uncertainty intensifies. Building upon these observations, we provide a threshold for quantitative analysis. Notably, to ensure a security performance loss below 10%, when the channel uncertainty is 0.3 or lower, a choice of $B = 3$ is adequate. However, when the uncertainty escalates to 0.6, a value of $B = 5$ is suggested. Therefore, after making a trade-off, we can obtain that the greater resolution B is necessary to keep the performance loss in a certain range as CSI uncertainty increases. This underscores the practicality of adopting a finite-resolution phase shifter setting in the RIS-aided mmWave system for optimal performance.

7. Conclusion

In this work, we investigated the secure transmission under the effect of the non-neglectable practical issues in a mult-RIS-aided mmWave system, including the high computational complexity, imperfect CSI acquisition, and finite resolution phase shifters limitation. A robust PLS enhancement method was proposed to solve the challenging optimization problem due to the coupled variables, complex functions, non-convex constraints, and uncertain system states. Both theoretical derivations and simulations demonstrated that the proposed algorithms could mitigate the joint negative effects of practical issues and outperform the benchmark schemes in convergence. Moreover, it was illustrated that there exists a tradeoff between secure performance and complexity/overhead, which can help multiple RIS deployments potentially be extended to more practical secure communication scenarios.

Acknowledgments

This work was supported in part by the National Key R&D Program of China (No. 2020YFB1805000), the National Natural Science Foundation of China (NSFC) under Grant 61871070, 91938202, and the Sichuan Science and Technology Program under Grant 2022YFG0005.

References

[1] K. Sakaguchi, G.K. Tran, H. Shimodaira, S. Nanba, T. Sakurai, K. Takinami, I. Siaud, E.C. Strinati, A. Capone, I. Karls, R. Arefi, and T. Haustein, "Millimeter-wave evolution for 5g cellular networks," IEICE Trans. Commun., vol.E98-B, no.3, pp.388–402, March 2015.

[2] K. Ishibashi, T. Hara, S. Uchimura, T. Iye, Y. Fujii, T. Murakami, and H. Shinbo, "User-centric design of millimeter wave communications for beyond 5G and 6G," IEICE Trans. Commun., vol.E105-B, no.10, pp.1117–1129, Oct. 2022.

[3] X. Ge, R. Zi, X. Xiong, Q. Li, and L. Wang, "Millimeter wave communications with OAM-SM scheme for future mobile networks," IEEE J. Sel. Areas Commun., vol.35, no.9, pp.2163–2177, 2017.

[4] A. Almohamad, A.M. Tahir, A. Al-Kababji, H.M. Furqan, T. Khattab, M.O. Hasna, and H. Arslan, "Smart and secure wireless communications via reflecting intelligent surfaces: A short survey," IEEE Open J. Commun. Soc., vol.1, pp.1442–1456, 2020.

[5] A. Mukherjee, S.A.A. Fakoorian, J. Huang, and A.L. Swindlehurst, "Principles of physical layer security in multiuser wireless networks: A survey," IEEE Commun. Surveys Tuts., vol.16, no.3, pp.1550–1573, 2014.

[6] L. Dong, Z. Han, A.P. Petropulu, and H.V. Poor, "Improving wireless physical layer security via cooperating relays," IEEE Trans. Signal Process., vol.58, no.3, pp.1875–1888, 2010.

[7] J. Zhu, R. Schober, and V.K. Bhargava, "Linear precoding of data and artificial noise in secure massive MIMO systems," IEEE Trans. Wireless Commun., vol.15, no.3, pp.2245–2261, 2016.

[8] E. Tekin and A. Yener, "The general Gaussian multiple-access and two-way wiretap channels: Achievable rates and cooperative jamming," IEEE Trans. Inf. Theory, vol.54, no.6, pp.2735–2751, 2008.

[9] L. Hu, H. Wen, B. Wu, F. Pan, R. Liao, H. Song, J. Tang, and X. Wang, "Cooperative jamming for physical layer security enhancement in Internet of things," IEEE Internet Things J., vol.5, no.1, pp.219–228, 2018.

[10] X. Yu, D. Xu, Y. Sun, D.W.K. Ng, and R. Schober, "Robust and secure wireless communications via intelligent reflecting surfaces," IEEE J. Sel. Areas Commun., vol.38, no.11, pp.2637–2652, 2020.

[11] C. Liaskos, S. Nie, A. Tsioliaridou, A. Pitsillides, S. Ioannidis, and I.F. Akyildiz, "A new wireless communication paradigm through software-controlled metasurfaces," IEEE Commun. Mag., vol.56, no.9, pp.162–169, 2018.

[12] M. Zhao, Q. Wu, M. Zhao, and R. Zhang, "Exploiting amplitude control in intelligent reflecting surface aided wireless communication with imperfect CSI," CoRR, vol.abs/2005.07002, 2020.

[13] Q. Wu and R. Zhang, "Intelligent reflecting surface enhanced wireless network: Joint active and passive beamforming design," IEEE Global Communications Conference, GLOBECOM 2018, Abu Dhabi, United Arab Emirates, pp.1–6, 2018.

[14] P. Wang, J. Fang, X. Yuan, Z. Chen, and H. Li, "Intelligent reflecting surface-assisted millimeter wave communications: Joint active and passive precoding design," IEEE Trans. Veh. Technol., vol.69, no.12, pp.14960–14973, 2020.

[15] H. Shen, W. Xu, S. Gong, Z. He, and C. Zhao, "Secrecy rate maximization for intelligent reflecting surface assisted multi-antenna communications," IEEE Commun. Lett., vol.23, no.9, pp.1488–1492, 2019.

[16] X. Yu, D. Xu, and R. Schober, "Enabling secure wireless communications via intelligent reflecting surfaces," 2019 IEEE Global Communications Conference, GLOBECOM 2019, Waikoloa, HI, USA, pp.1–6, 2019.

[17] K. Feng, X. Li, Y. Han, S. Jin, and Y. Chen, "Physical layer security enhancement exploiting intelligent reflecting surface," IEEE Commun. Lett., vol.25, no.3, pp.734–738, 2021.

[18] F. Karim, B. Hazarika, S.K. Singh, and K. Singh, "A performance analysis for multi-ris-assisted full duplex wireless communication system," IEEE International Conference on Acoustics, Speech and Signal Processing, ICASSP 2022, Virtual and Singapore, pp.5313–5317, 2022.

[19] W. Mei and R. Zhang, "Performance analysis and user association optimization for wireless network aided by multiple intelligent reflecting surfaces," IEEE Trans. Commun., vol.69, no.9, pp.6296–6312, 2021.

[20] Y. Ogawa, T. Utsuno, T. Nishimura, T. Ohgane, and T. Sato, "Subterahertz MIMO spatial multiplexing in indoor propagation environments," IEICE Trans. Commun., vol.E105-B, no.10, pp.1130–1138, Oct. 2022.

[21] A. Alkhateeb, J. Mo, N. González Prelcic, and R.W. Heath, Jr., "Mimo precoding and combining solutions for millimeter-wave systems," IEEE Commun. Mag., vol.52, no.12, pp.122–131, 2014.

[22] J.A. Zhang, X. Huang, V. Dyadyuk, and Y.J. Guo, "Massive hybrid antenna array for millimeter-wave cellular communications," IEEE Wirel. Commun., vol.22, no.1, pp.79–87, 2015.
[23] S.A. Busari, K.M.S. Huq, S. Mumtaz, L. Dai, and J. Rodriguez, "Millimeter-wave massive MIMO communication for future wireless systems: A survey," IEEE Commun. Surveys Tuts., vol.20, no.2, pp.836–869, 2018.
[24] Y. Cao, T. Lv, and W. Ni, "Intelligent reflecting surface aided multi-user mmWave communications for coverage enhancement," 31st IEEE Annual International Symposium on Personal, Indoor and Mobile Radio Communications, PIMRC 2020, London, United Kingdom, pp.1–6, 2020.
[25] S. Gong, C. Xing, P. Yue, L. Zhao, and T.Q.S. Quek, "Hybrid analog and digital beamforming for RIS-assisted mmWave communications," IEEE Trans. Wireless Commun., vol.22, no.3, pp.1537–1554, 2023.
[26] Y. Xiu, J. Zhao, C. Yuen, Z. Zhang, and G. Gui, "Secure beamforming for multiple intelligent reflecting surfaces aided mmWave systems," IEEE Commun. Lett., vol.25, no.2, pp.417–421, 2021.
[27] K. Yamaguchi, H.P. Bui, Y. Ogawa, T. Nishimura, and T. Ohgane, "Channel prediction techniques for a multi-user MIMO system in time-varying environments," IEICE Trans. Commun., vol.E97-B, no.12, pp.2747–2755, Dec. 2014.
[28] L. Wei, C. Huang, G.C. Alexandropoulos, C. Yuen, Z. Zhang, and M. Debbah, "Channel estimation for RIS-empowered multi-user MISO wireless communications," IEEE Trans. Commun., vol.69, no.6, pp.4144–4157, 2021.
[29] H. Liu, X. Yuan, and Y.A. Zhang, "Matrix-calibration-based cascaded channel estimation for reconfigurable intelligent surface assisted multiuser MIMO," IEEE J. Sel. Areas Commun., vol.38, no.11, pp.2621–2636, 2020.
[30] G. Zhou, C. Pan, H. Ren, K. Wang, and A. Nallanathan, "A framework of robust transmission design for IRS-aided MISO communications with imperfect cascaded channels," IEEE Trans. Signal Process., vol.68, pp.5092–5106, 2020.
[31] D. Yang, J. Xu, W. Xu, Y. Huang, and Z. Lu, "Secure communication for spatially correlated RIS-aided multiuser massive MIMO systems: Analysis and optimization," IEEE Commun. Lett., vol.27, no.3, pp.797–801, 2023.
[32] H. Niu, X. Lei, Y. Xiao, M. Xiao, and S. Mumtaz, "On the efficient design of RIS-assisted secure MISO transmission," IEEE Wireless Commun. Lett., vol.11, no.8, pp.1664–1668, 2022.
[33] Z. Zhang, C. Zhang, C. Jiang, F. Jia, J. Ge, and F. Gong, "Improving physical layer security for reconfigurable intelligent surface aided NOMA 6G networks," IEEE Trans. Veh. Technol., vol.70, no.5, pp.4451–4463, 2021.
[34] X. Lu, W. Yang, X. Guan, Q. Wu, and Y. Cai, "Robust and secure beamforming for intelligent reflecting surface aided mmWave MISO systems," IEEE Wireless Commun. Lett., vol.9, no.12, pp.2068–2072, 2020.
[35] L. Zhang, C. Pan, Y. Wang, H. Ren, and K. Wang, "Robust beamforming design for intelligent reflecting surface aided cognitive radio systems with imperfect cascaded CSI," IEEE Trans. Cogn. Commun. Netw., vol.8, no.1, pp.186–201, 2022.
[36] W. Wang, W. Ni, H. Tian, Z. Yang, C. Huang, and K. Wong, "Safeguarding NOMA networks via reconfigurable dual-functional surface under imperfect CSI," IEEE J. Sel. Topics Signal Process., vol.16, no.5, pp.950–966, 2022.
[37] H. Jia, L. Ma, and S. Valaee, "STAR-RIS enabled downlink secure NOMA network under imperfect CSI of eavesdroppers," IEEE Commun. Lett., vol.27, no.3, pp.802–806, 2023.
[38] Z. Li, S. Wang, M. Wen, and Y. Wu, "RIS-aided secure energy-efficiency maximization under uncertain CSI," IEEE Global Communications Conference, GLOBECOM 2022, Rio de Janeiro, Brazil, pp.4637–4642, 2022.
[39] S. Li, B. Duo, M.D. Renzo, M. Tao, and X. Yuan, "Robust secure UAV communications with the aid of reconfigurable intelligent surfaces," IEEE Trans. Wireless Commun., vol.20, no.10, pp.6402–6417, 2021.
[40] C. Liu, C. Tian, and P. Liu, "RIS-assisted secure transmission exploiting statistical CSI of eavesdropper," IEEE Global Communications Conference, GLOBECOM 2021, Madrid, Spain, pp.1–6, 2021.
[41] Q. Wu, S. Zhang, B. Zheng, C. You, and R. Zhang, "Intelligent reflecting surface-aided wireless communications: A tutorial," IEEE Trans. Commun., vol.69, no.5, pp.3313–3351, 2021.
[42] G. Zhou, C. Pan, H. Ren, K. Wang, and Z. Peng, "Secure wireless communication in RIS-aided MISO system with hardware impairments," IEEE Wireless Commun. Lett., vol.10, no.6, pp.1309–1313, 2021.
[43] H. Guo, Y. Liang, J. Chen, and E.G. Larsson, "Weighted sum-rate maximization for reconfigurable intelligent surface aided wireless networks," IEEE Trans. Wireless Commun., vol.19, no.5, pp.3064–3076, 2020.
[44] F. Sohrabi and W. Yu, "Hybrid digital and analog beamforming design for large-scale antenna arrays," IEEE J. Sel. Topics Signal Process., vol.10, no.3, pp.501–513, 2016.
[45] Q. Wu and R. Zhang, "Beamforming optimization for wireless network aided by intelligent reflecting surface with discrete phase shifts," IEEE Trans. Commun., vol.68, no.3, pp.1838–1851, 2020.
[46] B. Di, H. Zhang, L. Song, Y. Li, Z. Han, and H.V. Poor, "Hybrid beamforming for reconfigurable intelligent surface based multi-user communications: Achievable rates with limited discrete phase shifts," IEEE J. Sel. Areas Commun., vol.38, no.8, pp.1809–1822, 2020.
[47] Y. Cao, T. Lv, and W. Ni, "Intelligent reflecting surface aided multi-user mmWave communications for coverage enhancement," 31st IEEE Annual International Symposium on Personal, Indoor and Mobile Radio Communications, PIMRC 2020, London, United Kingdom, pp.1–6, 2020.
[48] H. Zhang, B. Di, L. Song, and Z. Han, "Reconfigurable intelligent surfaces assisted communications with limited phase shifts: How many phase shifts are enough?," IEEE Trans. Veh. Technol., vol.69, no.4, pp.4498–4502, 2020.
[49] A. Almohamad, A.M. Tahir, A. Al-Kababji, H.M. Furqan, T. Khattab, M.O. Hasna, and H. Arslan, "Smart and secure wireless communications via reflecting intelligent surfaces: A short survey," IEEE Open J. Commun. Soc., vol.1, pp.1442–1456, 2020.
[50] Z. Li, W. Chen, Q. Wu, H. Cao, K. Wang, and J. Li, "Robust beamforming design and time allocation for IRS-assisted wireless powered communication networks," IEEE Trans. Commun., vol.70, no.4, pp.2838–2852, 2022.
[51] M.R. Akdeniz, Y. Liu, M.K. Samimi, S. Sun, S. Rangan, T.S. Rappaport, and E. Erkip, "Millimeter wave channel modeling and cellular capacity evaluation," IEEE J. Sel. Areas Commun., vol.32, no.6, pp.1164–1179, 2014.
[52] D. Shiu, G.J. Foschini, M.J. Gans, and J.M. Kahn, "Fading correlation and its effect on the capacity of multielement antenna systems," IEEE Trans. Commun., vol.48, no.3, pp.502–513, 2000.
[53] K. Xu, J. Zhang, X. Yang, S. Ma, and G. Yang, "On the sum-rate of ris-assisted MIMO multiple-access channels over spatially correlated rician fading," IEEE Trans. Commun., vol.69, no.12, pp.8228–8241, 2021.
[54] H. Gao, P.J. Smith, and M.V. Clark, "Theoretical reliability of MMSE linear diversity combining in Rayleigh-fading additive interference channels," IEEE Trans. Commun., vol.46, no.5, pp.666–672, 1998.
[55] A.D. Dabbagh and D.J. Love, "Multiple antenna MMSE based downlink precoding with quantized feedback or channel mismatch," IEEE Trans. Commun., vol.56, no.11, pp.1859–1868, 2008.
[56] B. Zheng and R. Zhang, "Intelligent reflecting surface-enhanced OFDM: channel estimation and reflection optimization," IEEE Wireless Commun. Lett., vol.9, no.4, pp.518–522, 2020.
[57] S.P. Boyd and L. Vandenberghe, Convex Optimization, Cambridge University Press, 2014.

[58] K. Shen and W. Yu, "Fractional programming for communication systems — Part II: Uplink scheduling via matching," IEEE Trans. Signal Process., vol.66, no.10, pp.2631–2644, 2018.
[59] D.P. a. Bertsekas, Nonlinear Programming, 2nd ed., Athena Scientific Belmont, Athena Scientific, MA, USA, 1999.
[60] Y. Xu and W. Yin, "A block coordinate descent method for regularized multiconvex optimization with applications to nonnegative tensor factorization and completion," SIAM J. Imaging Sci., vol.6, no.3, pp.1758–1789, 2013.
[61] M. Razaviyayn, M. Hong, and Z. Luo, "A unified convergence analysis of block successive minimization methods for nonsmooth optimization," SIAM J. Optim., vol.23, no.2, pp.1126–1153, 2013.
[62] A. Liu, V.K.N. Lau, and M. Zhao, "Online successive convex approximation for two-stage stochastic nonconvex optimization," IEEE Trans. Signal Process., vol.66, no.22, pp.5941–5955, 2018.
[63] W. Shi, X. Zhou, L. Jia, Y. Wu, F. Shu, and J. Wang, "Enhanced secure wireless information and power transfer via intelligent reflecting surface," IEEE Commun. Lett., vol.25, no.4, pp.1084–1088, 2021.

Qingqing Tu received the B.Eng. and M.Eng. degrees in Computer Science and Engineering from the University of Electronic Science and Technology of China (UESTC) in 2011 and 2014, respectively. She has also completed an international exchange study in the University of Electro-Communications in Japan. She is currently working toward the Ph.D. degree in cyberspace security with the University of Electronic Science and Technology of China and serving with the National Computer Network Emergency Response Technical Team/Coordination Center of China. Her research interests include physical layer security and millimeter wave communications.

Zheng Dong received the B.Sc. (in Electronic Information Science and Engineering) and M.Eng. (in Communication and Information System) degrees from the School of Information Science and Engineering, Shandong University, Jinan, China, in 2009 and 2012, respectively, and the Ph.D. degree from the Department of Electrical and Computer Engineering (in Telecommunications), McMaster University, Canada, in 2016. He was a Postdoc Research Fellow in the School of Electrical and Information Engineering, The University of Sydney, Australia. He is currently a Professor in the School of Information Science and Engineering, Shandong University, China. His research interests include the Industrial Internet of Things and Ultra-reliable Low-Latency Communications.

Xianbing Zou received the B.Eng. degree in Physics at Gannan Normal University, Ganzhou, China, in 1995, and M.Eng. degree in Electromagnetic Field and Microwave Technology at the University of Electronic Science and Technology of China (UESTC), Chengdu, China, in 1998. He is now an associate professor of Electronics and Communication Engineering at the National Key Laboratory of Science and Technology on Communications, UESTC. His current research interests are in RF front-end and hardware platform of wireless communication system.

Ning Wei received the B.Eng. and Ph.D. degrees in electrical engineering from the University of Electronic Science and Technology of China (UESTC) in 2003 and 2008, respectively. He was a Visitor of The University of Texas at Austin, Austin, TX, USA, in 2012. He is currently a Full Professor with the University of Electronic Science and Technology of China. His research interests include wireless communications networks and signal processing, including ad hoc networks, multiRAT, channel coding, millimeter wave communications, cooperative communications, and physical-layer network coding. He has served as a Reviewer for various international journals and conferences, including the IEEE TRANSACTIONS ON VEHICULAR TECHNOLOGY and the IEEE TRANSACTIONS ON WIRELESS COMMUNICATIONS.